KU LEUVEN

FACULTY OF SCIENCE

Bistability & Traveling Front Dynamics in the Cell Cycle Regulator Protein, Aurora B Kinase

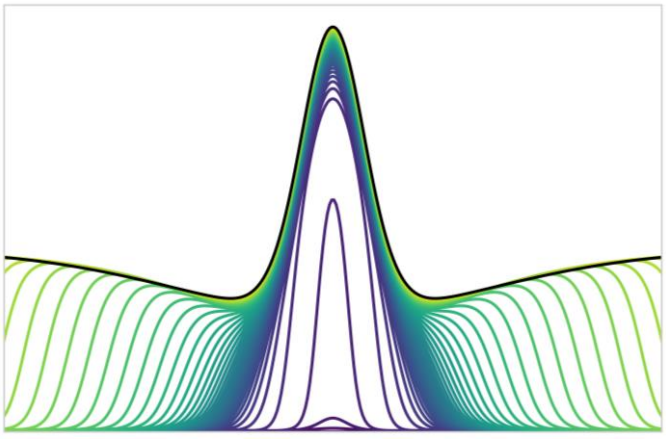

Patrick Govoni

Supervisor: Prof. Lendert Gelens

Affiliation: *Department of Cellular and Molecular Medicine*

Group: *Dynamics in Biological Systems*

Thesis presented in
fulfillment of the requirements
for the degree of Master of Science
in Biochemistry & Biophysics

Academic year 2020-2021

Contents

1. Summary for Scientific Audience

Reliable chromosome segregation is vital to an organism's long-term survival. Aurora B kinase, one of the key players in this critical mitotic event, uses a spatial gradient in activity to help selectively stabilize kinetochore-microtubule attachments and achieve properly balanced biorientation before chromatid splitting in anaphase. A popular theory asserts that Aurora B achieves this spatial gradient through the combination of localization, diffusion, and bistable reaction kinetics together with phosphatase. In this report I will discuss the individual aspects of these components in a theoretical context, the experimental effort to construct a minimal kinase-phosphatase system, as well as simulation explorations of the system using two different modeling approaches.

2. Summary for General Audience

During the process in which cells grow and divide, an organism's DNA must be replicated and equally divided between cells. One particular enzyme, Aurora B kinase, plays a major role in ensuring an equal quantity of DNA ends up in the two divided cells. Aurora B activates in a spatially confined way such that the structure involved in pulling the replicated DNA apart is effectively and equally stabilized before splitting. A popular argument claims that this spatial behavior arises due to Aurora B fixing itself to a central part along DNA strands by binding to particular molecules, its local movement when not fixed, and a particular nonlinear phenomenon arising from reaction with itself and its inhibitor, phosphatase. In this report I will discuss the individual aspects of these three components, the experimental effort to construct a cell-free kinase-phosphatase system, as well as simulation explorations of the system using two different perspectives.

3. Introduction

3.1. Mitosis

Self-replication is a phenomenon at the heart of what defines life. With life comes death, and a living entity is defined by its ability to replicate itself in order to sustain the timescale of its relevance. This is true for individual organisms as it is for individual cells within multicellular organisms. Eukaryotes, a type of organism whose cells contain nuclei (animals inclusive), evolved a particular means of replicating its cells in what is called the cell cycle[1].

The eukaryotic cell cycle can be split into two main stages: interphase and the mitotic phase[2]. Interphase contains three phases: G1, S, and G2[2]. DNA is duplicated in S or synthesis phase[2]. The other two phases (G for gap) involve checkpoints where the cell decides whether or not to divide or copy its DNA [2]. Interphase is where a cell spends most of its time – growing, producing protein, and duplicating its major organelles in preparation for division[3].

The mitotic phase, split into mitosis and cytokinesis, is the busy period where the cell is undergoing separation and division[1]. Mitosis can be split into five phases: prophase, prometaphase, metaphase, anaphase, and telophase, schematically illustrated in Figure 1[1,4].

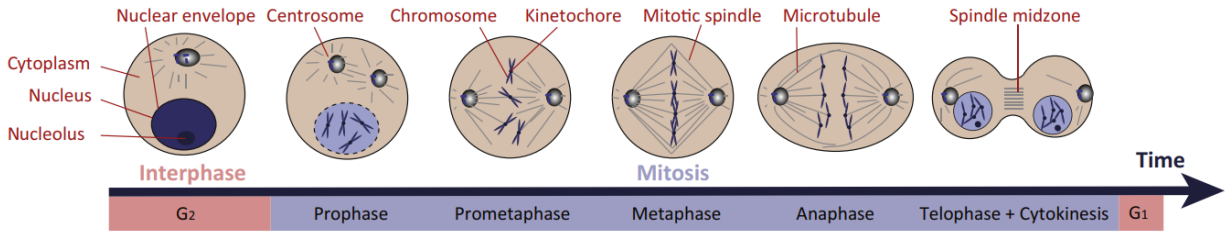

Figure 1: Diagram of the phases and major components in the cell cycle (reprinted from Box 1, Gelens, 2018).

During prophase, the duplicated strands of DNA (chromosomes) condense into tightly packed, X-shaped structures[1]. The two identical copies (sister chromatids) each make up one side of the 'X' and are connected in the center at a point called the centromere[3]. In animal and yeast cells, a structure called the mitotic spindle starts to form in this stage. The spindle is made up of microtubules, polymers of protein involved in structure and transport, and is responsible for separating the two chromatids[1]. The organelles involved in organizing these spindle microtubules, centrosomes in animal cells, move to the opposite sides (poles) of the cell to begin to form the spindle[1].

Following prophase, prometaphase is when the nuclear membrane breaks down and protein structures called kinetochores form around the centromeres[1]. The microtubules emerging from the centrosomes reach out and attach to the kinetochores[1]. Motor proteins along the microtubules exert a pulling force on the attached chromosomes toward their respective centrosomes[5]. Unequal attachment results in unequal forces, causing the chromosomes to be pulled toward the cell pole with the greater number of attached microtubules[5]. This stage is associated with a high rate of microtubule turnover in order to reduce the number of erroneous attachments[6].

Moving onto metaphase, chromosomes eventually line up along the cell equator via the balance of forces between microtubules[1]. Regulatory error-correction fixes mismatched combinations of kinetochores and microtubules and their resulting tension[6]. During this stage microtubule turnover

decreases and correct attachments are stabilized[6]. The cell then passes what is called the spindle assembly checkpoint when forces are properly balanced and attachments are stabilized, where the chromosomes achieve biorientation[6].

After passing the checkpoint, anaphase is when the sister chromatids are split at the centromere and are pulled toward the opposite poles of the cell[1]. The regulation in the previous stage ensures that each pole and eventually each daughter cell ends up with the same number of chromosomes[6,7].

Telophase and cytokinesis then complete mitosis by reversing processes from early mitosis and physically dividing the cell[3]. The nucleus reassembles around the pulled chromatids, which decondense into their more functionally available form[1]. The spindle disassembles and the long spindle microtubules depolymerize[3]. Actin microfilaments and motor proteins then generate a contractile force to cleave the cell into two daughter cells, finishing the self-replication process of the cell cycle[1].

3.2. Aurora B Kinase Function & Regulation

A critical step in mitosis is ensuring balanced, bioriented kinetochore-microtubule attachments in each chromosome before separation[7]. If this step were to fail and the chromosomes were to unequally segregate between the two daughter cells, a condition termed aneuploidy, the cell could experience reduced fitness or elicit tumorigenesis[7]. Therefore, chromosomal regulation requires robust control for long-term organism survival. Aurora B kinase is one of the key regulator proteins responsible for controlling chromosomal segregation though the regulation of kinetochore-microtubule attachment stability and the spindle assembly checkpoint[8]. Before we discuss the specifics of what Aurora B kinase does, let's walk through what a kinase is and how it works.

Kinases are a type of enzymatic protein that catalyzes a type of biochemical switch, activating, inactivating, or otherwise altering the function of another molecule[9]. Specifically, they catalyze the transfer of a phosphate group from an energy source such as ATP to its target, the substrate[9]. This transfer or modification is called phosphorylation[9]. A key aspect that makes this switch so useful is that it is reversible[9]. Phosphatases, another enzymatic protein, catalyze the reverse reaction, dephosphorylation[9]. Kinases and phosphatases work together in concert across time and space to orchestrate complex responses to a plethora of signals, from cell differentiation to mitosis[9].

Regarding mitosis, Aurora B kinase regulates kinetochore-microtubule attachment stability by phosphorylating substrates in the outer kinetochore thereby reducing their binding affinity toward microtubules[6]. While high Aurora B activity ensures high turnover in early mitosis, activity reduces in late mitosis, thus increasing attachment stability[6]. A popular theory is that this change in activity is partly due to the increased tension and distance between the two kinetochores when under biorientation and partly due to a spatial gradient in Aurora B activity that develops from the combination of its localization, diffusion, and reaction properties[6,10].

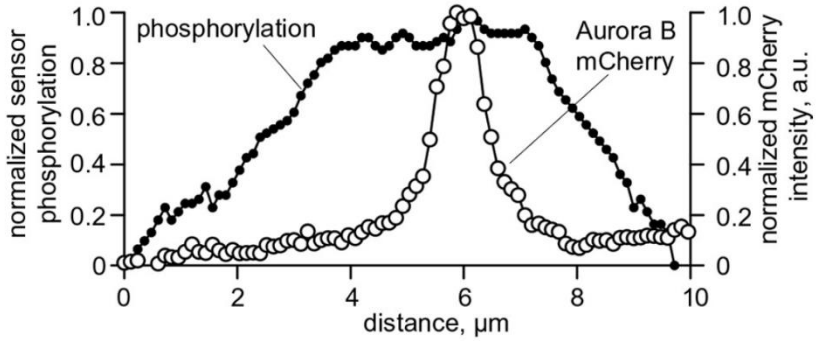

Figure 2: Spatial patterns in Aurora B localization and resulting phosphorylation gradient, taken in the anaphase of HeLa cells. Localization imaged via Aurora B-mCherry sensor and plotted as white circles. Phosphorylation imaged via chromatin-targeted FRET sensor and plotted as black circles (reprinted from Fig. 1A, Zaytsev, 2016).

During different stages of the cell cycle, Aurora B is recruited to specific locations in the cell through an array of interactions[6,8,11,12]. Aurora B is part of the chromosomal passenger complex (CPC) along with inner centromere protein (INCENP), Survivin, and Borealin which play critical roles in the localization and regulation of Aurora B[11]. In interphase, before mitosis, the CPC is initially targeted to the nucleus via heterochromatin protein 1[11]. The phosphorylated histone H3 then recruits the CPC to the inner centromere during prophase just before nuclear membrane breakdown[8]. Finally in anaphase, when the chromosomes are starting to be pulled apart, the CPC delocalizes to the spindle midzone[12]. The overall localization along a chromosome in anaphase as measured via a fluorescent sensor is plotted in Figure 2[10].

Despite localization to the inner centromere, Aurora B develops a long-range, sharply defined gradient in activity by the end of prophase, when the chromosomes begin to align and local CPC concentration rises, and lasts through anaphase[13,14]. The result of the activity gradient, the spatial profile of phosphorylated substrate, is shown in Figure 2[10]. Perturbing this gradient has been shown to disrupt mitotic progression, indicating that this spatial organization is vital[14]. The currently dominant theory suggests the gradient in Aurora B activity and therefore kinetochore-microtubule attachment stability is a regulatory mechanism that complements the tension from pulling spindle microtubules[6,15]. As the kinetochores are pulled away from each other, they enter a region of low Aurora B activity and thus stabilize their attachments with spindle microtubules, as summarized in Figure 3[6].

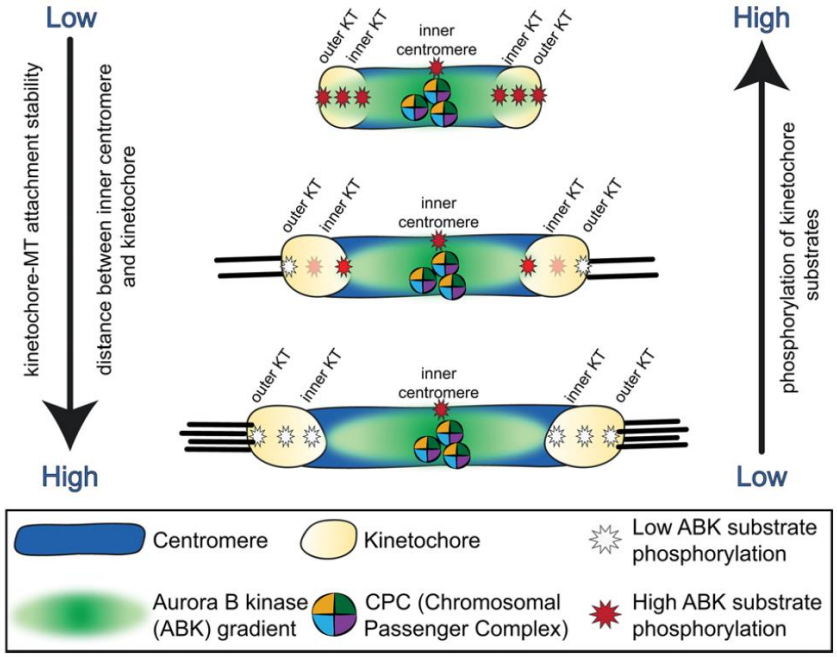

Figure 3: Proposed mechanism for regulating chromosomal biorientation through the combination of tension, which pulls the kinetochores apart from each other, and a spatial gradient in Aurora B kinase activity, which controls kinetochore-microtubule attachment stability. (Reprinted from Figure 2, Broad, 2020).

There have been several theories put forth as to how Aurora B activity extends beyond its localization to its substrates at the kinetochores[6,8,11]. One theory posits that extension from INCENP's flexible single α-helix domain is enough to create a spatially constrained zone of activity[6]. The more popular theory suggests diffusion of activated kinase to be responsible for the spatial activity gradient[14,16,17]. However it is argued that diffusion alone would likely not be able to explain the sharp spatial gradient that can recognize the difference in distance between kinetochores when under different tension loads, a distance as little as 50-100 nm[10]. Zaytsev et al proposed a nonlinear reaction component in addition to diffusion to explain this complex spatial organization and used a purified component system to demonstrate their theory[10].

Aurora B is activated via a nonlinear pathway through interaction with INCENP, which could be the mechanism behind the long-range sharply defined spatial activity gradient. The activation has been shown to occur both in cis and in trans[10]. This is a biological way of saying Aurora B can activate itself and once activated, it can activate other Aurora B in a positive feedback loop. This second pathway, the in trans feedback loop, causes the nonlinearity which has been argued as responsible for forming the activity gradient required for establishing stable kinetochore-microtubule attachments[10,18]. How these localization, diffusion, and nonlinear reaction components combine to form the spatial gradient in Aurora B activity is the biological basis of this thesis.

3.3. Thesis Goals & Report Structure

The original goal of the thesis was to first reproduce the spatial activity gradient in the Aurora B kinase-phosphatase system responsible for controlling chromosome separation in mitosis, both experimentally and via simulation, and then to change experimental conditions and expand the theory. As will be shown in this report, the goal shifted a couple times throughout this period. The first shift was due to a change in personal preference away from an experimental focus and towards simulation. The second shift occurred once it was found that the nonlinear phenomenon that had been published as being responsible for the spatial gradient was, in fact, not. At this point two choices were presented: to change the model to properly describe the spatial gradient or to change parameters in order to explore the unique interplay between reaction, diffusion, and localization forces. We chose the latter, and I will walk you through this decision in the following three sections outlining the results of the thesis.

The first section will be discussing the nonlinear reaction network underlying the Aurora B system. The activation and inactivation kinetics of Aurora B kinase and an interesting nonlinear phenomena called bistability that emerges within particular ranges of kinase and phosphatase concentrations will be major topics. I will also introduce the two central model approaches used with respect to reaction kinetics: mass-action and phenomenological. At this point in the report, the system I discuss is well-mixed and any spatial effects are left for a later section. The section will largely be a review of fundamental concepts well known in dynamical systems as it pertains to the Aurora B kinase-phosphatase system and is meant to introduce the subject for you, the reader.

In the next section I will go through the principles behind and results of experiments performed. The experimental setup involves expression of minimal system components in order to study the essence of the kinase-phosphatase system without extraneous interactions. This cell-free approach eliminates significant barriers to understanding biological design, including the difficult-to-penetrate cell wall, reactive components complicating an interaction network, and issues related with cell viability[19]. Once bistability in this minimal system could be reproduced as per the results published by Zaytsev et al[10], the

plan was to perturb the system and observe effects. Varying temperature, or thermal noise, could be interesting as to how it affects bistable behavior. Using kinase sourced from different organisms, different phosphatases, as well as altering the spatial localization were also directions considered. However, due to a change in personal preference midway through the project, attention was diverted away from experimental aspects and instead toward the theoretical arena.

The final section of the results will step through simulation explorations that resulted from adding diffusion and localization to bistable kinetics. I will start with an attempt to produce a spatial phenomenon called traveling fronts that emerge from the interplay between bistable reaction dynamics and diffusion using the biological diffusion speed. I will then argue that these phenomena are not relevant on the length scale of chromosomes and thus could not be the underlying cause of the spatial gradient in mitosis. Instead, discussion will shift to a more interesting region of the reaction-diffusion system where unique spatial behavior can be observed. The mass-action model is initially used to produce a curious stalling behavior involving localization at reduced diffusion speeds, which is then analyzed in greater detail using the simpler, phenomenological model. Geometric-based analysis is employed to explain and reproduce this behavior, as well as to investigate the value of particular parameters in the system. Using intuition gathered from this analysis, the mass-action model will be used to investigate the role of kinase and phosphatase dynamics and altered binding site profiles to local and global behavior.

The report will then summarize and conclude the key findings from the results of the thesis. The following section will provide outlook to potential future directions extending the work completed. The next section includes the theoretical and experimental methods with details needed to reproduce the results within the thesis. A section for references and one for supplemental figures follow. Supplemental movies central to providing intuitive understanding of a few concepts are added to the digital version of the report.

4. Modeling the Biochemical Reaction Kinetics and Bistability of an Aurora B Kinase-Phosphatase System

This section serves as an introduction to several essential concepts underpinning the reaction kinetics of the Aurora B kinase-phosphatase system as well as the two major models used for simulation.

4.1. Activation & Inactivation

Bistability requires two critical components: a nonlinear feedback loop and a balancing between states[20]. Aurora B kinase activation consists of an in cis as well as an in trans pathway, as shown in Figure 4A[10]. The in trans activation of Aurora B via phosphorylation is a positive feedback loop, which is inherently nonlinear and is dominant relative to the in cis pathway. At low Aurora B activation, each molecule that is activated can then activate more molecules, and the effect is amplification or exponential behavior, shown by the orange curve in Figure 4B. At high Aurora B activation, each activated molecule decreases the pool of available inactivated kinase, giving rise to asymptotic behavior. The combination of the two results in an S-shaped or sigmoidal curve, which can be seen in other nonlinear feedback loops such as cooperative genetic or protein interactions where the Hill coefficient is greater than 1 or in strong Allee effect population dynamics[20,21]. This contrasts with the hyperbolic response of the in cis pathway, the system without positive feedback, represented as the blue curve in Figure 4B.

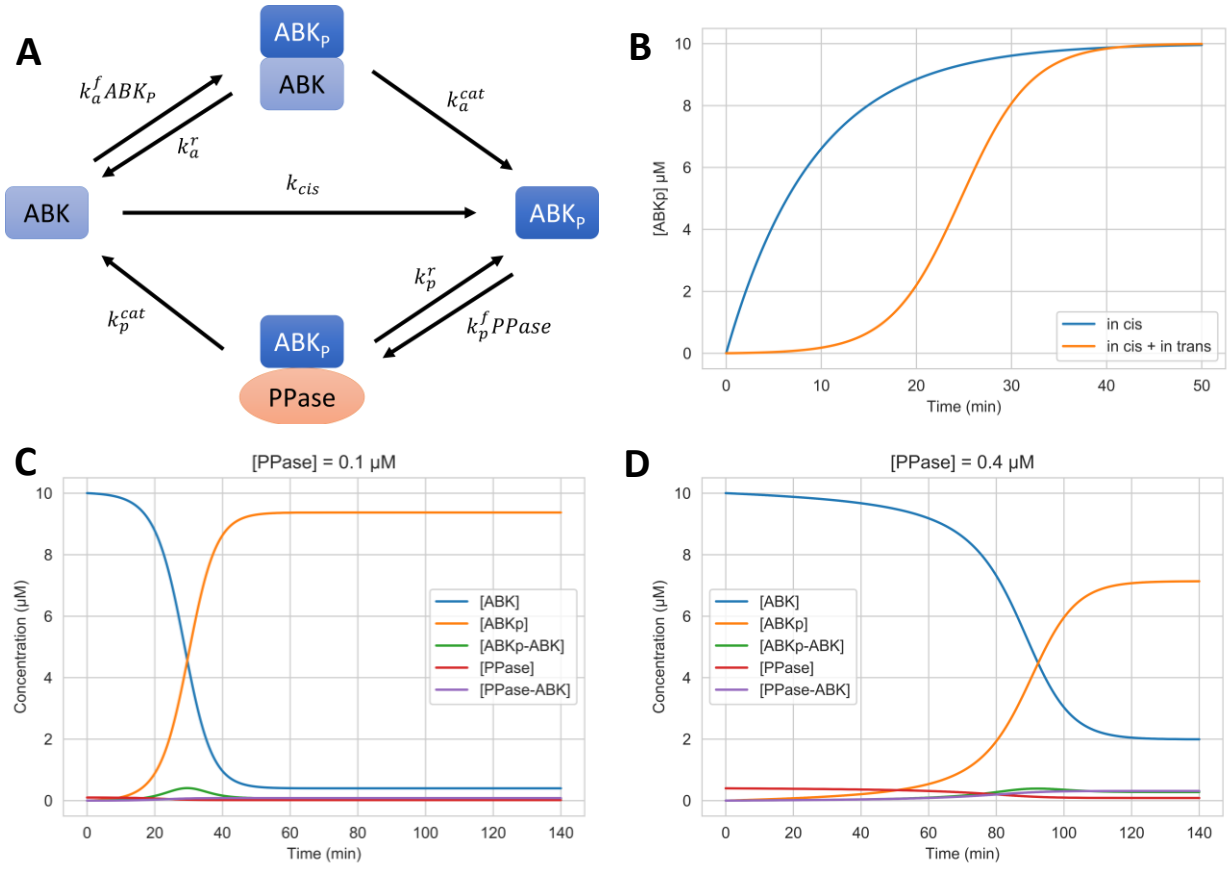

Figure 4: Activation-Inactivation of Aurora B Kinase. (A) Diagram of the mass-action reaction model. ABK: Aurora B kinase, ABKp: phosphorylated/activated Aurora B kinase, PPase: phosphatase. Reaction rates are specified in Methods. (B) Comparing Aurora B activation rates of an in cis pathway and of a pathway with an in trans (nonlinear, positive feedback) reaction term included. (C) Activation dynamics of all system components in a system with 0.1 µM phosphatase and (D) 0.4 µM phosphatase.

Inactivation of Aurora B via phosphatase provides the opposing force that balances the activation as a negative feedback loop. In Figures 4C/D, we can see that increasing the amount of phosphatase results in a decrease in the effective force of activation: activation time increases, maximum activation rate decreases, and final activated, or steady state, concentration decreases.

4.2. Bistability

By balancing nonlinear activation feedback and inactivation, bistability can be achieved[20]. At particular kinase and phosphatase concentrations, the positive and negative feedback loops are close enough to each other in strength such that low or high initial activated Aurora B concentrations will cause the system to stay in a low or high steady state of activation. This is demonstrated by the pair of trajectories in Figure 5A with a phosphatase concentration of 0.35 µM, where an initially low state retains inactivity while an initially high state retains activity. This dependence on history imposes memory function to the system[22,23]. In other phosphatase concentrations, one loop is dominant to the extent that any initial activated Aurora B concentration will be pushed to one particular, monostable state. The importance of the nonlinear feedback loop to bistability can be seen by contrasting this system with a system without feedback, Figure 5B shows purely monostable behavior given the same inputs.

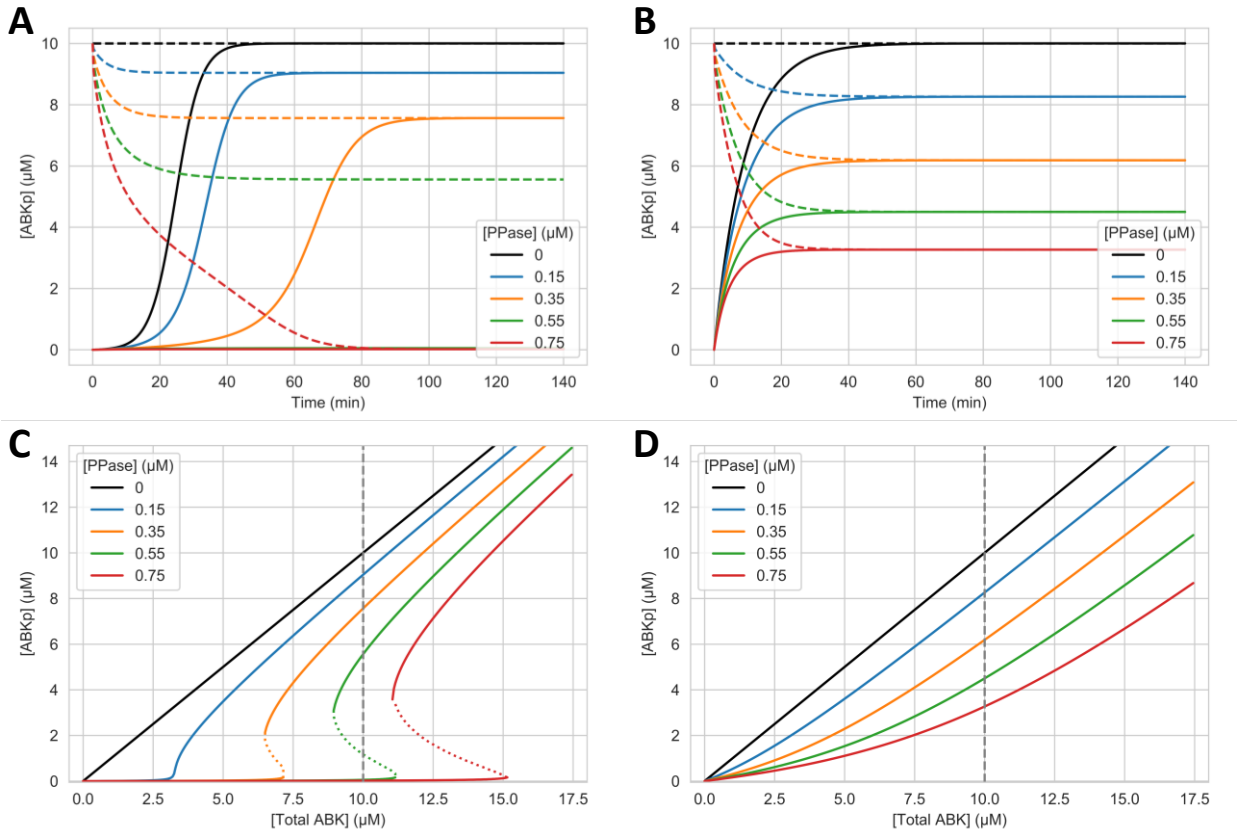

Figure 5: Bistability in Aurora B Kinetics. (A) Time simulation of Aurora B activation at different phosphatase concentrations with the nonlinear feedback loop (B) and without. The solid lines start at an inactive state where there is no active Aurora B, the dashed lines start at an active state where all Aurora B in the system is active. (C) Steady state activated Aurora B kinase concentrations with respect to total kinase and phosphatase concentrations with the nonlinear feedback loop (D) and without. The dashed gray lines in (C/D) relate these figures to the system with 10 µm total kinase in (A/B).

A comprehensive picture of the feedback balancing can clearly be seen by taking the final or stable steady states of the previously described time simulations and plotting these in relation to the input variables of total kinase and phosphatase concentration. As can be seen in Figure 5C, bistability for the system with in trans feedback exists at particular kinase and phosphatase combinations, where both high and low steady states are possible for the same set of parameters. Extending the comparison with the in cis system without feedback, Figure 5D shows monostability at all parameter combinations. The dashed gray line in each figure relates the steady states found in Figures 5A/B to this graphical representation, highlighting the bistability in the system with nonlinear feedback at 0.35 µM phosphatase.

At low phosphatase, say at 0.15 µM, system behavior manifests as a type of critical thresholding. Low kinase concentration does not result in activation, and past a certain amount, the activation reattains its linear nature as when phosphatase is absent. This can be explained by the difference in binding affinities activated kinase has for the phosphatase inactivation loop relative to the in trans activation feedback loop, described elsewhere as inhibitor ultrasensitivity[24]. Since K_M for the inactivation reaction is lower than for the activation reaction, the active kinase prefers binding to phosphatase than to inactive kinase. Essentially at low kinase concentrations, active kinase is 'soaked up' by the available phosphatase in the system, inhibiting autoactivation, in other words the kinase is blocked from activating itself. That is, until a threshold is reached that exceeds this inhibition or soaking by the phosphatase, where any extra free active kinase then stimulates its positive feedback loop and exponential behavior, leading to the high steady state.

As phosphatase increases, this inactive steady state begins to extend beyond the leftmost part of the top branch. Between these two monostable branches, a space termed the bistable region and bounded by two saddle-node bifurcations, a bistability threshold can be defined, shown by the dotted lines[25]. If a system lies above this threshold, it will activate, and if below, it will inactivate. This is commonly visualized as a pair of potential energy wells, illustrated in Figure 6, where a hypothetical ball will roll into either depending on which side it starts with respect to the threshold[25]. Once at either well, or state, the system requires energy to reach the other side of the bistable region and switch states, a behavior called hysteresis[20]. In this sense, a bistable system can be seen as a kind of noise filter or checkpoint, only allowing perturbations that can pass the threshold, or roll over the hill between wells, to switch states[23].

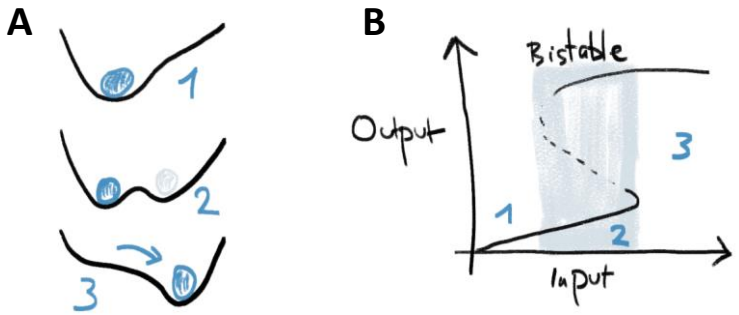

Figure 6: Monostability & Bistability: (A) as a pair of potential energy wells (B) and in the phase space. (Reprinted from Fig. 1, Rombouts, 2021).

Why this bottom branch extends past the top branch at higher phosphatase concentrations can be explained by the competing nature of kinase and phosphatase. As previously mentioned, activation behavior at low active kinase levels is exponential, which is by nature slow to start. Phosphatase present in the system will preferably bind to any active kinase and if levels are high enough, will eliminate the signal. On the other hand, if the system starts with high active kinase levels, the asymptotic nature of this part of the activation curve can be strong enough to withstand the inactivation force of the phosphatase.

4.3. Mass-Action & Phenomenological Models

Two main models were used to simulate Aurora B kinase dynamics: mass-action and phenomenological. Whereas the more complicated, empirical mass-action model was used to observe complex phenomena with more realistic and experimentally relevant kinetics (Figure 4A), the simpler, phenomenological model was used to explain and analyze underlying processes (Figure 7). The mass-action approach regards multiple molecule complexes as components separate from free Aurora B molecules, the binding processes as forward and reverse reactions, and product formation as a one-way catalytic step. Whereas the phenomenological approach uses Michaelis-Menten constants to describe both binding and product formation, and uses Hill coefficients to describe nonlinear activity. Although this approach is less accurate, its reduction of the number of differential equations of the system from eleven to one greatly facilitates analysis. The equations are shown below:

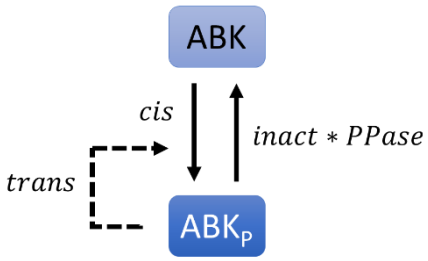

Figure 7: Diagram of a phenomenological simplification of the Aurora B kinase-phosphatase system.

$$\frac{dA}{dt} = r(A) + D\frac{d^2A}{dx^2}$$

$$r(A) = \left(cis + trans * \frac{A^n}{K_f^n + A^n}\right)(A_{tot} - A) - \left(inact * P * \frac{K_r^m}{K_r^m + A^m}\right)A$$

where A is the concentration of active Aurora B kinase, $r(A)$ is the net activation rate, A_{tot} is the total amount of kinase, and P is the concentration of phosphatase. The constants $trans$, $inact$, K_f, and K_r are all set to one for simplicity. The constant cis is set to 0.01 to reflect the large difference between in cis and in trans reaction rates, as in the mass-action model. The Hill coefficient n is raised to 2 while m is kept at one to reflect nonlinear activation and linear inactivation.

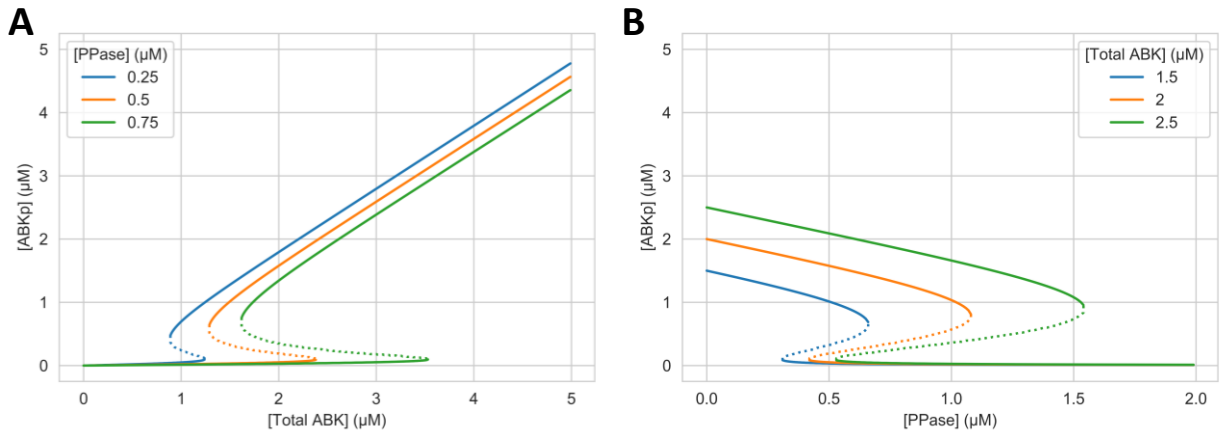

Figure 8: Bistability curves with respect to (A) changing total kinase and (B) changing phosphatase concentrations as modeled using the phenomenological model. Although the model can quickly and simply reproduce fundamental behavior, precise values and relationships found using this approach will not be as experimentally relevant as the mass-action model.

The phenomenological model can recreate the same phenomena in the mass-action model, Figures 8A/B demonstrate the balance between the activation and inactivation feedback loops via their plotting their steady states. As phosphatase is increased while total kinase is kept constant, the bottom branch of the bistability curve lengthens relative to the top branch, showing the increase in relative strength of the negative feedback loop. As total kinase is increased while phosphatase is kept constant, the opposite occurs. While this model was not tuned to approximate the values in the mass-action model, the critical behavior can be reproduced. Using the phenomenological model takes much less computational power and time as well as reducing the number of dynamically changing variables, facilitating analysis.

5. Experimental Reconstruction of a Minimal Aurora B Kinase-Phosphatase System

The following section steps through both the principles and results of experiments performed with the initial goal of generating a purified quantity of Aurora B kinase. Or rather, to express and purify the minimal component of Aurora B along with the minimal component of INCENP required for Aurora B activation. Following purification, the plan was to combine the kinase with phosphatase in different amounts and activation states in order to first reproduce bistability and then to change the system and observe related effects. However, the direction was shifted before purification was completed due to a change in personal preference towards simulation.

5.1. Plasmids

Aurora B kinase and the INbox domain of INCENP, the portion required to activate Aurora B, were encoded into short circular strands of DNA (plasmids) in order to be introduced into bacterial cells and produced (expressed). Two plasmids were modified by the genetic information (sequences) for each protein. One with protein sequences originating from Xenopus laevis and one from a human source. A diagram of how the plasmids were constructed is shown in Figure 9[26]. The plasmids were received from outside labs, courtesy of the Grishchuk and Aleyde labs, respectively. As pGEX-6P-2 plasmids, expression of the protein sequences was regulated via lac operator and lacI repressor[26]. The lacI protein, produced from its gene in the plasmid, binds to the lac operator in the vicinity of the tac promoter, allowing expression of the downstream Aurora B and INbox only when IPTG is added to the bacteria[26]. Downstream of the promoter and lac operator is the expressed protein sequence[26]. Specific to pGEX-6P-2 plasmids, the expressed protein is attached to a glutathione S-transferase (GST) tag which is later used in purification, and is cleavable via PreScission protease[26]. An ampicillin resistance gene is included as well that allows bacterial growth in ampicillin, an antibiotic, only when the plasmid has successfully been inserted into the bacteria's genome[26].

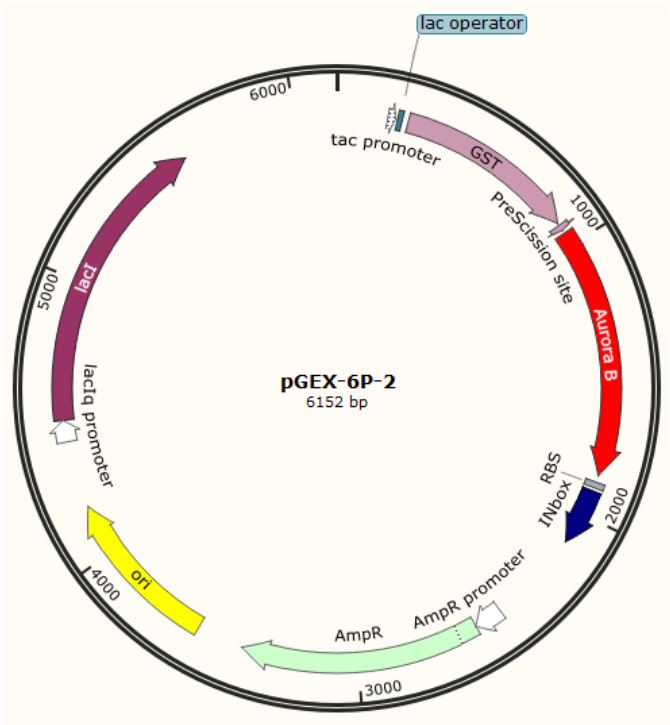

Figure 9: Plasmid construction for the dual expression of GST-tagged Aurora B kinase and the INbox of INCENP.

5.2. Amplification & Sequencing

The plasmids were first amplified and sent for DNA sequencing to validate the protein sequences contained. Amplification is bacterial transformation with a fast-growing bacterial strain with the goal of expanding plasmid concentration[27]. Transformation is the term describing insertion of a plasmid into the genome of an organism, E. coli bacteria in our case[27]. It is a multi-step process which starts by

introducing the plasmid into bacterial cells via heat shock[27]. A sudden temperature increase permeabilizes the bacterial membrane, which then allows the plasmid to be passed into the cell[27]. This has a moderate success rate, and growing these heat shocked cells in ampicillin-rich media selectively allows only the successfully transformed bacteria to grow due to the ampicillin-resistance gene in the plasmid[27]. The transformed bacteria are picked and grown in larger volumes to amplify the number of copies of plasmid.

After amplifying the Aurora B-INbox plasmids, the genetic material was extracted using a EZLA DNA Mini Kit and sent to LGC Genomics to be sequenced. The sequences of the proteins for each plasmid were aligned using Snapgene. Relating the sequences to literature found that both plasmids contained the minimal sequences required for Aurora B kinase binding with INbox and activation[28]. Comparing the sequences from X. laevis with those from humans, it was found that the two retain conserved interactions despite sequence differences between organisms[29]. It was also found that the sequences for the two proteins were separated by a ribosome binding site and would thus be expressed as separate proteins.

5.3. Transformation & Expression

The two plasmids were then transformed into a second bacterial cell optimized for the expression of transformed protein using a similar procedure as described above. Expression of the Aurora B kinase and INbox was triggered by the addition of IPTG. The quantity of protein expressed was measured via western blot.

Western blot is a rapid, semi-quantitative assay which uses antibodies to detect proteins. First, the cells containing the expressed proteins are lysed and the proteins are degraded in a reducing buffer[30]. This allows the proteins to be separated by their molecular weight rather than their native conformation of charge[30]. Next, the sample undergoes a process called gel electrophoresis, which starts in the buffer[30]. Negatively charged sodium dodecyl sulfate binds to the denatured proteins at a ratio of one molecule per two amino acid residues, thus imparting a particular charge-to-mass ratio to the protein[30]. The samples are loaded into a polyacrylamide gel which is subjected to an electrical charge, causing the negatively charged protein complexes to travel towards the positive electrode at the bottom of the gel[30]. Once the proteins are sufficiently separated along the gel, the proteins are transferred to a solid PVDF membrane, or blot, using electrophoresis with the positive electrode placed behind the membrane[30]. The open parts of the membrane that do not contain transferred protein are blocked by a milk solution in order to reduce non-specific antibody binding, otherwise it would be difficult to discern the protein on the membrane[30]. The blocked membranes are incubated with primary then secondary antibodies that are set to detect a representative part of the expressed protein, GST in our case. The primary antibody is specific to a particular group but is not directly detectable whereas the secondary recognizes the primary antibody and is detectable[30]. Finally, the proteins are visualized via a process called electrochemiluminescence where enzymes conjugated to the secondary antibodies emit light as they react to an added substrate[30]. The light is then recorded over a period of time to derive images that can be used to determine approximate quantities of proteins, separated in space by the separate wells of the gel and by the molecular weight and corresponding distance traveled via electrophoresis[30].

Transformation and expression of the two Aurora B kinase and INbox plasmids were successful, as shown in the western blot in Supplemental Figure 1. Human and Xenopus protein complexes both revealed bands in the expected areas and agreed in relative positioning with each other. Positive controls were

run in order to verify the success of various parts of the protocol. GST, the positive control for antibody binding, showed a band in the expected area. This verifies that the antibody was present in adequate amounts and performed as anticipated. A third plasmid was run as a positive control for transformation and also gave an anticipated signal. This plasmid was known in the lab for its ease of transformation and expression, if this band was present but the bands for the Aurora B – INbox plasmids were not, it would have indicated an issue with transformation and expression of those plasmids in particular.

Transformation of both plasmids was repeated with larger batch sizes for purification. However the human plasmid transformation was unsuccessful as seen in the western blot in Supplemental Figure 2. The root cause is not known and likely repeat runs would elucidate the problem. A successful transformation of PreScission protease, an ingredient needed for the final step of purification, revealed a band in the expected area.

5.4. Purification

Purification of the expressed Aurora B and INbox protein complex and the PreScission protease was performed via affinity chromatography. This operation separates expressed protein via a specific, bindable tag, in our case the GST group attached to Aurora B[31]. After lysing cells that have expressed the protein via reducing buffer and sonication, lysate was incubated with glutathione beads and passed through a filtered column[31]. The tag then recognizes and binds to the glutathione. After a washing step, the glutathione-GST-protein complex was stripped from the beads in the column using free glutathione[31]. For the PreScission protease, this is the final purification step. For the Aurora B-INbox complex, the GST tag was removed by incubation with the GST-tagged PreScission protease[31]. This solution was passed again through a column containing glutathione beads but now the solution that passed through the column was collected since the cleaved protein complex no longer has its GST tag[31].

Measurement of expressed protein was performed in three different methods: Nanodrop, Bradford assay, and image analysis of a Coomassie gel. The Nanodrop measures absorbance at 280 nm specifically of the aromatic rings in typrophan and tyrosine, using the measurement to correlate molecular weight[32]. The Bradford assay uses a reaction of specific amino acid residues with the Coomassie Blue dye and a colorimetric method is used to associate the reacted dye with molecular weight[32]. Lastly, image analysis can be used with a Coomassie gel to relate a gradient of protein sample volumes to a gradient of standard protein volumes with known density such as BSA[33].

The purification of the PreScission protease was quite successful, generating a significant quantity of protease. The NanoDrop estimated an average protein concentration of 4.5 µg/µL (Supplemental Figure 3), however uncleaned protein from the surface of the instrument or the surfactant Triton-X100 could have affected this measurement. The Bradford assay estimated 9.7 µg/µL (Supplemental Figure 4), however this assay is compatible with glycerol concentrations of up to 10% whereas our sample had 60% glycerol. Finally, the Coomassie gel quantified the protein concentration at 15.6 µg/µL (Supplemental Figures 5-9). It is unclear which of these measurements were closest to the actual value without further testing.

Purification of the Aurora B – INCENP complex was unsuccessful, unfortunately. Protein aggregation was the likely cause, preventing passage through the filtered column and producing white tendrils extending below the filter. There were a few possibilities for root causes. The pelletized cells were allowed to stand at room temperature for over 20 minutes prior to transferring to the -80°C freezer, stimulating

aggregation. The protein amount could have simply been too much for the volumes we used, given the pre-purification western blot indicated a very high protein concentration. Or perhaps the salt concentration may have not been optimized for the protein complex. The relevant materials and data has been kept so that somebody who wishes to continue this project will be able to restart the project from here.

6. Modeling the Spatial Regulation and Traveling Front Dynamics of an Aurora B Kinase-Phosphatase System

This last results section extends the theoretical underpinnings of the bistable reaction kinetics introduced in Section 4 into the spatial dimension with diffusion and localization. It begins by an introduction into the core concepts of diffusion, traveling fronts, and localization. The section will walk through traveling front dynamics at a biological diffusion speed, highlighting a key issue with the relevance of traveling fronts on a chromosomal length scale with the fast biological diffusion speed, and the research direction shift to a lower diffusion speed. Using the mass-action and phenomenological models as well as geometric-based analysis, the section will observe and explain interesting spatiotemporal phenomena of kinase-phosphatase dynamics.

6.1. Diffusion & Traveling Fronts

The behavior of bistable systems in space can give rise to phenomena known as traveling fronts or spatial waves[4]. It is this concept that has been theorized as the potential underlying mechanism that shapes sharply defined spatial Aurora B activity gradients in mitosis[10]. Whereas simple diffusion results in spatial gradients that lose amplitude and speed with time (Figure 10A), diffusion coupled with bistability can result in traveling fronts constant in both amplitude and speed (Figure 10B)[4]. This transforms an equalization force, diffusion, into a force for information propagation where the constant amplitude

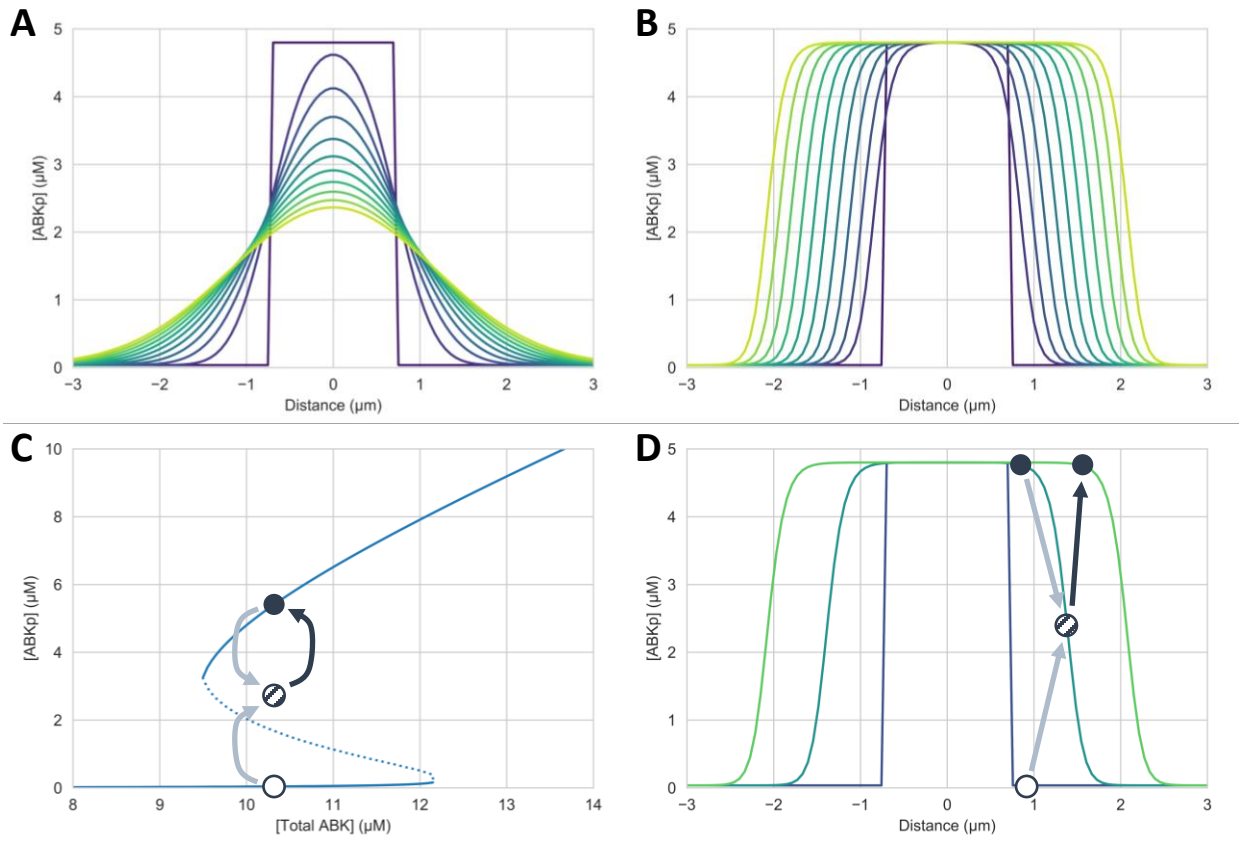

Figure 10: Traveling Front Dynamics. (A) Diffusion of an activated Aurora B kinase perturbation without reaction. (B) A traveling front: diffusion with a bistable reaction component. (C) Mechanistic diagram of traveling front propagation with respect to the bistability curve (D) and its spatial analog.

characteristic ensures a signal equally transfers from source to recipient. Traveling fronts can be seen in several systems involving information propagation, ranging from intracellular calcium waves and neurons to population dynamics and liquid crystals[34-37].

In a bistable traveling front, there are two spatially defined states separated by a boundary or transition region. Between the two states there is diffusion into the transition region which pushes local concentration to a level above or below the bistability threshold. If this point is above the threshold for an adequate amount of time, the traveling front will be activating from the low to the high steady state and spreading outwards, shown in Figures 10C/D. If below, the traveling front will be inactivating and contracting. This transition can be more formally derived via geometric-based analysis, and will be a discussion later in this report (Section 6.6).

6.2. Localization

In addition to reaction and diffusion, localization plays an important role in mediating Aurora B activity by defining the origin of spatial gradient[10]. During metaphase, Aurora B has been found to bind to chromosomes with highest concentration at the centromere and a lower concentration along the chromosome arms[38] (Figure 11B[10]). Kinase binds or unbinds at certain rates regardless of activity, and most other reaction parameters stay the same regardless of whether the kinase is in the bound or diffusing state, as proposed by Zaytsev et al[10] (Figure 11A). Only the rate of complex formation between two bound kinase is reduced to account for steric hindrance[10]. The spatial heterogeneity of the binding sites stimulates kinase movement towards the centromere, which can result in a centromeric autoactivating region and a traveling front which propagates along the chromosome arms. How this can emerge will be discussed in later in this report (Section 6.5).

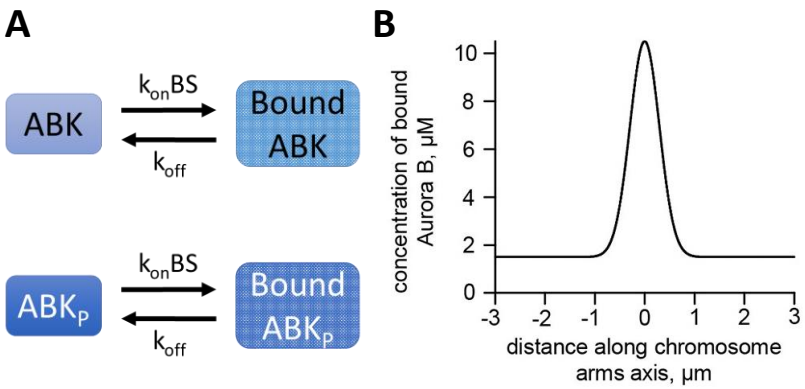

Figure 11: Localization of Aurora B. (A) Diagram of binding/unbinding reactions. (B) Concentration profile of Aurora B binding sites along a chromosome (reprinted from Fig. 6 - Supplement 1C, Zaytsev, 2016).

A critical aspect to consider here is the relevant length scale of a chromosome, approximately 6 µm. As shown back in Figure 2, the anaphase gradient in phosphorylation which correlates Aurora B activity, extends from a low to high state on the same length scale. This point is made pertinent in the following section, where we will compare this length scale with that of simulated traveling front gradients.

6.3. Traveling Fronts in the Mass-Action Model with Biological Diffusion Speed (1 $\mu m^2/s$)

The initial aim of simulating the spatial aspects of the bistable kinase-phosphatase system was to reproduce traveling front behavior using the model from the paper by Zaytsev et al[10]. A key figure and concept from the paper demonstrates linear front propagation speed, a characteristic of bistable

traveling fronts[4]. The figure, reprinted as Figure 12A, concerned only the reaction and diffusion aspects of the system without the localization effect from kinase binding. The plot describes a linear activation or phosphorylation speed of a front in the model containing bistability at 1 µm/min and contrasts this with a model without bistability. No kinase or phosphatase parameters were given, nor was it described what perturbation was given to the system. Here a perturbation refers to a spatially limited area with activated initial conditions contrasting with inactive initial conditions in the surrounding area. A perturbation is necessary in a bistable system due to its history-dependence. A fully inactive or active area will stay in that condition unless a perturbation pushes the system state in the other direction.

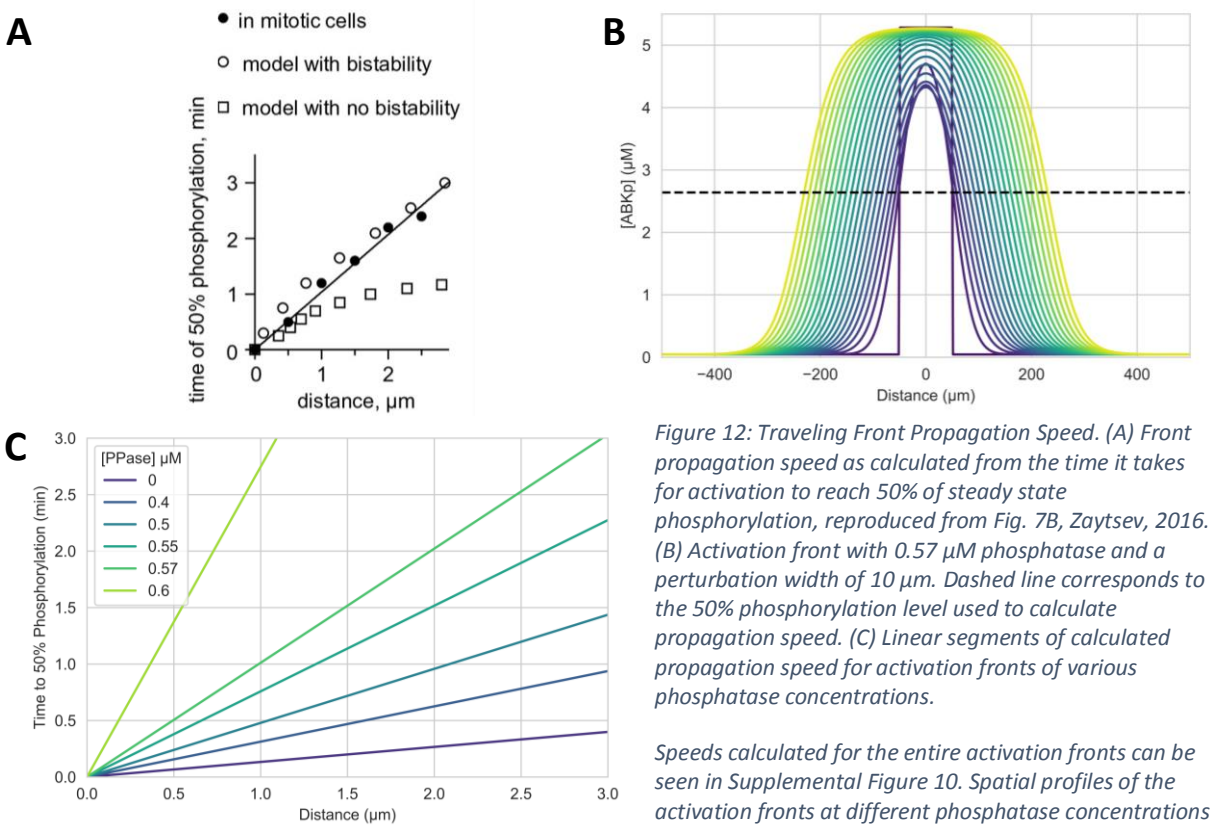

Figure 12: Traveling Front Propagation Speed. (A) Front propagation speed as calculated from the time it takes for activation to reach 50% of steady state phosphorylation, reproduced from Fig. 7B, Zaytsev, 2016. (B) Activation front with 0.57 µM phosphatase and a perturbation width of 10 µm. Dashed line corresponds to the 50% phosphorylation level used to calculate propagation speed. (C) Linear segments of calculated propagation speed for activation fronts of various phosphatase concentrations.

Speeds calculated for the entire activation fronts can be seen in Supplemental Figure 10. Spatial profiles of the activation fronts at different phosphatase concentrations are included as Supplemental Figure 11.

The perturbations used in order to calculate front propagation time were large enough to ensure a fully developed front with edges that extend from low to high steady state. One such figure is shown in Figure 12B, where the initial perturbation, the box in dark blue, quickly activates in a Gaussian-like shape of a traveling front. The time of 50% phosphorylation, the key metric in Figure 12A, was calculated by determining the time points at which each spatial slice reaches an activation level halfway between the low and high steady states, represented by the dashed line in Figure 12B. This constructs a curve that is linear across the range that a fully developed traveling front is progressing, and these curves are plotted for different phosphatase concentrations as Figure 12C. The nonlinear start and end to these curves were not plotted since these portions do not correspond to a fully developed traveling front. The full curves are printed as Supplemental Figure 10. The related front spatial profiles for the different phosphatase concentrations can be seen in Supplemental Figure 11. As can be seen in Figure 12C, phosphatase concentration strongly affects front propagation speed. The inverse slope of these curves describes speed in distance over time, thus we can see that low phosphatase results in a faster

propagation speed. This makes intuitive sense as phosphatase inhibits kinase activation and would thus slow down the speed at which it would activate and spread in the spatial dimension. It is possible to then conjecture that a phosphatase concentration of about 0.57 µM was used to plot the data in Figure 12A, especially given the sensitivity of curve slopes around 0.55 µM to 0.60 µM in Figure 12C.

However, although it was possible to recreate traveling fronts with linear propagation speed, the length scale of a fully developed front was an unexpected and major issue with this model. One of these fronts, roughly the latest time evolution of Figure 12B in yellow, extends hundreds of micrometers while a chromosome length is about 6 µm, as shown in Figures 2 and 7B. This can be also seen in other phosphatase concentrations as shown in Supplemental Figure 11. The issue can be visualized by zooming into Figure 12B and observing the span of 6 µm. The profile within that window would be nearly flat regardless of the state of the traveling front. Looking back to the measurements plotted in Figure 2, this is not what has been experimentally observed, where a sharp gradient can be seen spanning 3 µm. Decreasing the perturbation width from 100 µm to 10 µm does not change the global behavior for phosphatase concentrations below the bistable region and collapses perturbations within the bistable region, further highlighting the inadequacy of a bistable traveling front to explain interactions at this length scale (Supplemental Figure 12). At this point we can say that a bistable front as calculated using the reaction kinetics contained within this model cannot describe the spatial activity profile in mitosis. The potential causes to how a mistake could have been made by Zaytsev et al or to how the model may fail to adequately describe the interaction will be outlined in the conclusions (Section 7). Regardless, a bistable traveling front in this mass-action model is irrelevant on the length scale of a chromosome.

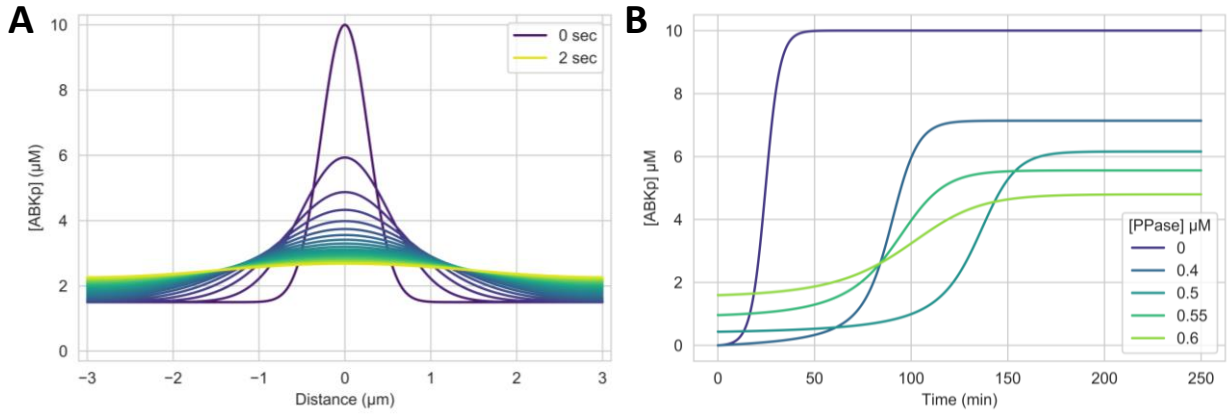

Figure 13: Diffusion vs. Activation Speed. (A) Diffusion of Aurora B from an initial condition equal to the binding site profile along a chromosome using a Fourier mesh to compute the spatial derivative across a spatial interval of 6 µm. (B) Aurora B activation with various phosphatase concentrations with a total kinase concentration of 10 µM and initial active kinase concentrations of zero or just above the bistable threshold for phosphatase concentrations within the bistable region, 0.5-0.65 µM shown in Supplemental Figure 13.

It was speculated that the cause of these extremely wide traveling fronts was that the diffusion speed of Aurora B is much faster than its activation speed. In Figure 13A, diffusion from an initial spatial distribution of a binding site profile as in Figure 7B takes about 2 seconds with the diffusion speed of 1 µm/s. This diffusion speed was calculated based on the previously determined measured Stokes radius of the CPC complex[10]. The diffusion calculations in these simulations were validated through the reproduction of a bistable traveling front in another recent paper[4] (Supplemental Figure 14). In Figure 13B, Aurora B activation from initial conditions of zero active kinase or at the bistable threshold for phosphatase concentrations within the bistable region of about 0.5 – 0.65 µM takes tens to hundreds of

minutes. These calculations were validated by reproducing a figure in the paper by Zaytsev et al (Supplemental Figure 15). Indeed, this comparison elucidates the vast timescale difference between diffusion and activation. To intuitively understand why this might lead to a wide front profile, strong diffusion pushes activated kinase out far before the slow activation can simulate its positive feedback loop and activate more kinase. Therefore the front that develops has a wide, shallow gradient. The diffusion speed was thus reduced to find the region in which diffusion and activation balanced to create a traveling front on the length scale of a chromosome.

6.4. Traveling Fronts in the Mass-Action Model with Reduced Diffusion Speed

The effect of shifting the balance between diffusion and activation speeds was first tested by creating traveling fronts via perturbation with localization not included. The length scale of the chromosome was assumed, the width of the binding sites, approximately 2 µm, was taken as the perturbation width, and a phosphatase concentration within the bistable region was used. As can be seen in Figure 14A, if diffusion is faster than reaction, perturbations will collapse before propagating (Figure 16A). In other words, diffusion pushes out active kinase before it can reach the bistability threshold in the vicinity and stimulate autoactivation. On the other end of the spectrum, if diffusion is much slower than reaction, perturbations will be stationary (Figure 16D). Within these two limits, a traveling front exists and the relative balance between diffusion and activation timescales determine its slope and propagation speed

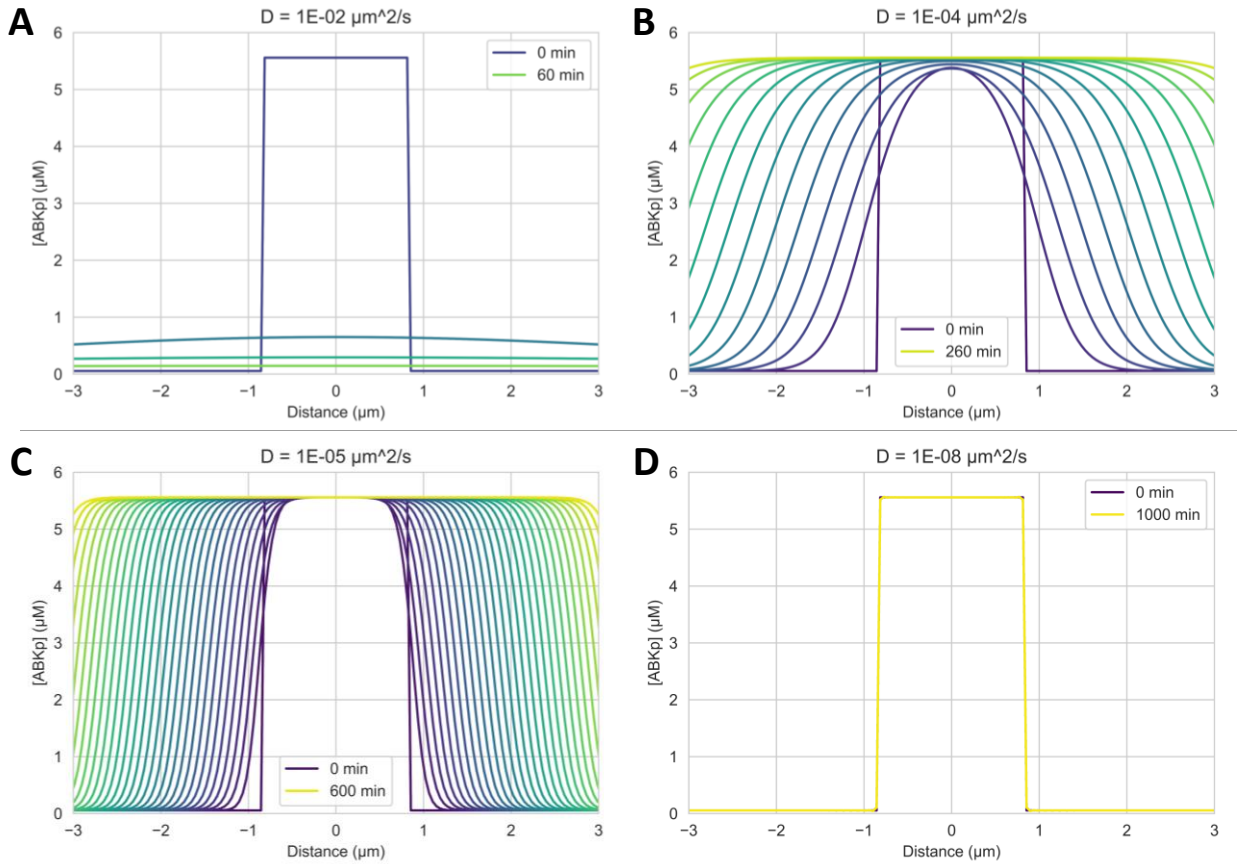

Figure 14: Effect of Varying Diffusion Speed on Traveling Front Behavior. From a diffusion speed much greater than reaction (A) to a diffusion speed much less than reaction (D). Each spatial profile is spaced 20 min from each other. Each simulation used 0.55 µM phosphatase and a spatial interval of 20 µm.

(Figures 16B/C). Activation behavior with the other intermediate diffusion speeds can be seen in Supplemental Figure 16. The behavior of a traveling front depends on local concentrations in the transition region between low and high steady states and their relation to the bistability threshold (Figure 10C), thus the relative balance of diffusion and activation timescales is critical.

While the lower diffusion speed within the approximate limits of 1E-2 and 1E-8 μm/s is necessary to produce traveling fronts in this Aurora B reaction system on the length scale of a chromosome, these lower diffusion speed is a departure from reality. Although the initial goal of the thesis was to recreate bistability and traveling front phenomena in the Aurora B system so as to bring our theoretical findings to the experimental system, the aim shifted here to observe these phenomena on a scale that better balances the interactions between reaction, diffusion, and localization.

By using a lower diffusion speed where diffusion and activation is balanced and the system produces a front gradient on the scale of a few micrometers, interesting spatial heterogeneity develops with respect to Aurora B localization to its chromosomal binding sites. The localization force uses a combination of diffusion and binding forces to spatially coordinate Aurora B towards the centromere. The Gaussian peak of centromeric binding sites introduces a heterogeneity in binding force, pulling in surrounding kinase so that the local centromeric concentration is greater than along the chromosome arms. As we have seen in Figures 5A and 5C, increased kinase concentrations along the monostable active steady state branch of the bistability curve results in autoactivation, even in the absence of perturbations given an initial condition of zero active kinase. Thus, the centromere pulls in surrounding kinase and autoactivates when its local concentration passes the edge of the bistable region of the bistability curve. Along the chromosome arms, however, the lower kinase concentration lies within the bistable region and requires diffusion of activated Aurora B from the centromeres in order to cross the bistability threshold and activate. In this sense, reactive dynamics with respect to the bistability curve becomes a local property. This spatially heterogeneous activation behavior can be seen as the temporal evolution of the spatial activation profile shown in Figure 15A. Here we see activation starting from centromere and progressing into a traveling front with a lower high steady state along the chromosome arms. The consistent amplitude of this traveling front seen as the flat tangent line along the arms emphasizes the information propagation aspect of bistable fronts. Another useful way to view this is to plot Aurora B activity as a heatmap and see the progression in both space and time, Figure 15C. Here we see the second aspect of traveling fronts, linear propagation speed, shown as the flat tangent line to the triangular shaped spatiotemporal gradient.

A curious property emerges at lower diffusion speeds where the transition between centromeric activation and front breakout along the arms is temporarily stalled. This is illustrated as the increased density of spatial profiles near the centrosome in Figure 15B and the shallow slope between chromosomal autoactivation and front breakout, about 150 and 1250 minutes respectively, in Figure 15D. This extended transition region indicates a transient minimum in the net force behind the reactive-diffusive traveling front. Further reduction of the diffusion speed fully can be described as fully reaching this minimum, pinning the activation front to the centromeric region (Supplemental Figure 16).

Front stopping, or pinning, has been observed in previously described reaction-diffusion systems though how exactly this behavior emerges have been rather specific to each system, with behavior originating from two species of differing diffusivities in a mass-conserved system[39], from inhibitor accumulation in a non-conserved excitable system[40], and from a spatially varying external activation source[21].

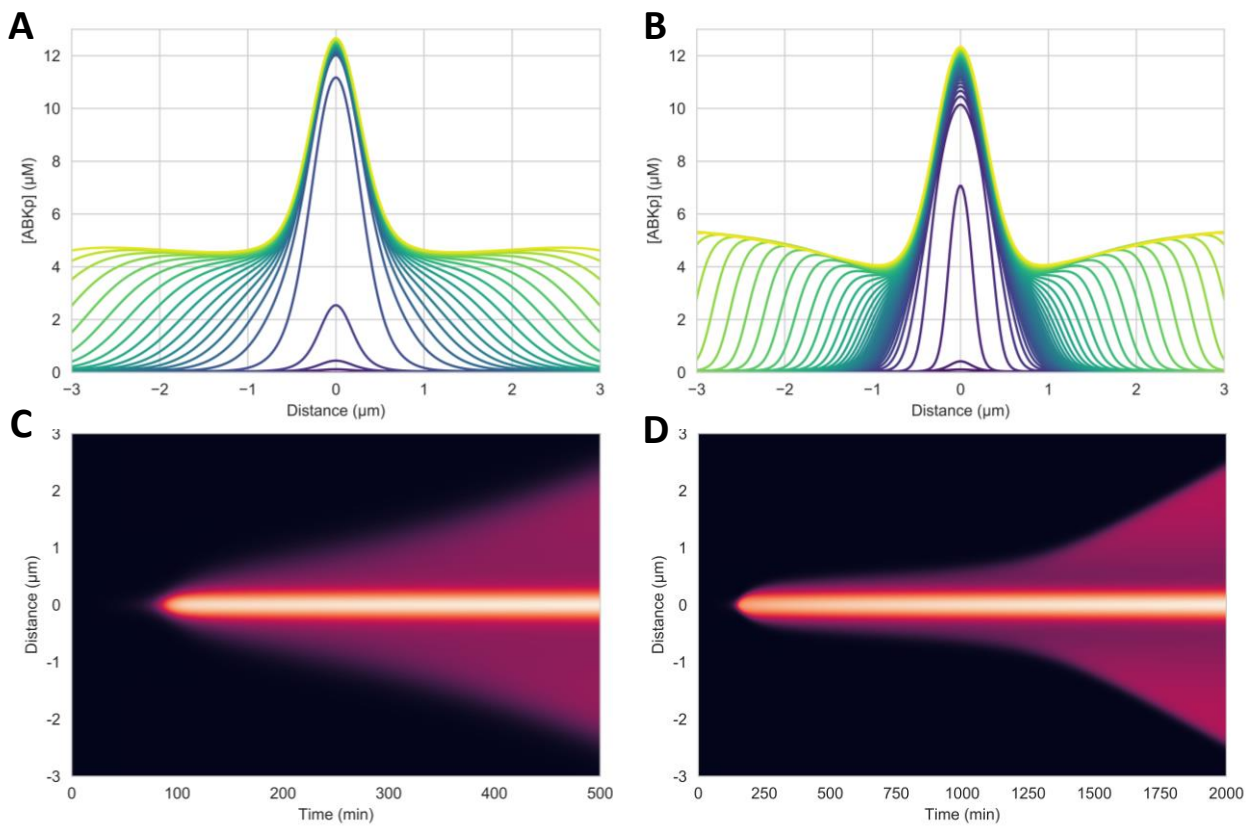

Figure 15: Traveling Fronts with Reduced Diffusion Speed. (A) Spatial activation profiles using diffusion speeds of 1E-4 μm²/s and (B) 10E-5 μm²/s. Corresponding heatmaps (C/D). Both simulations are with 0.55 μM phosphatase and a spatial interval of 10 μm.

The system in the first paper essentially couples the reaction and localization interactions found in our system. The two species balance between a diffusible, inactive form and a fixed, active form[39]. The front achieves a spatially distributed front through a positive feedback-mediated activation-localization, and is pinned to a single profile by reaching its appropriate energetic minimum regardless of initial conditions. Since our system decouples reaction and localization, their simplified principles do not directly apply.

The systems in the latter two papers include external source and degradation terms in their reaction kinetics and thus do not follow mass-conservation[21,40]. This key point as well as other aspects of their system sufficiently differentiate their system so as to not be directly applicable either. However, the system in the paper by Rulands et al describes a conceptual similarity to ours that sheds light on how to describe the stalling behavior in Figure 15B/D. Due to a gradient in external activation, the front in their system approaches a Maxwell point, referring to the thermodynamic Maxwell construction that designates distinct metastable states or phases near the liquid-vapor equilibrium[41,42]. In our system the two relevant phases are traveling fronts and stationary fronts. During a stalling transition, our front seems to approach this Maxwell point, or energetic equilibrium. Though whereas the system analyzed by Rulands et al concern a simple gradient in input, the equivalent in ours, kinase concentration, is dynamic in time as well as space.

In our mass-action model it is possible to observe this behavior, but the spatiotemporally dynamic kinase and phosphatase concentrations make it difficult to explain and analyze its origin. We will return to the mass-action model, but for now let us shift to a simplified model to better our intuition of the system.

6.5. Traveling Fronts in the Phenomenological Model

The phenomenological model can reproduce spatial phenomena in the mass-action model with some minor variations. Localization can be mimicked by using a spatially heterogeneous total kinase profile, the direct result of combined diffusion and localization. A profile similar to the binding site profile reproduces a traveling front as shown in Figures 16A/C/E. For cases in which the stalling behavior can be observed, Figures 16B/D/F, slow diffusion causes a transient valley of total kinase concentration between the centromere and chromosome arms. And for a certain range of reaction parameters, this results in a slow transition from centromeric activation to traveling front breakout. Faster diffusion will equalize the valleys before the front can reach this region or otherwise be able to activate the arms

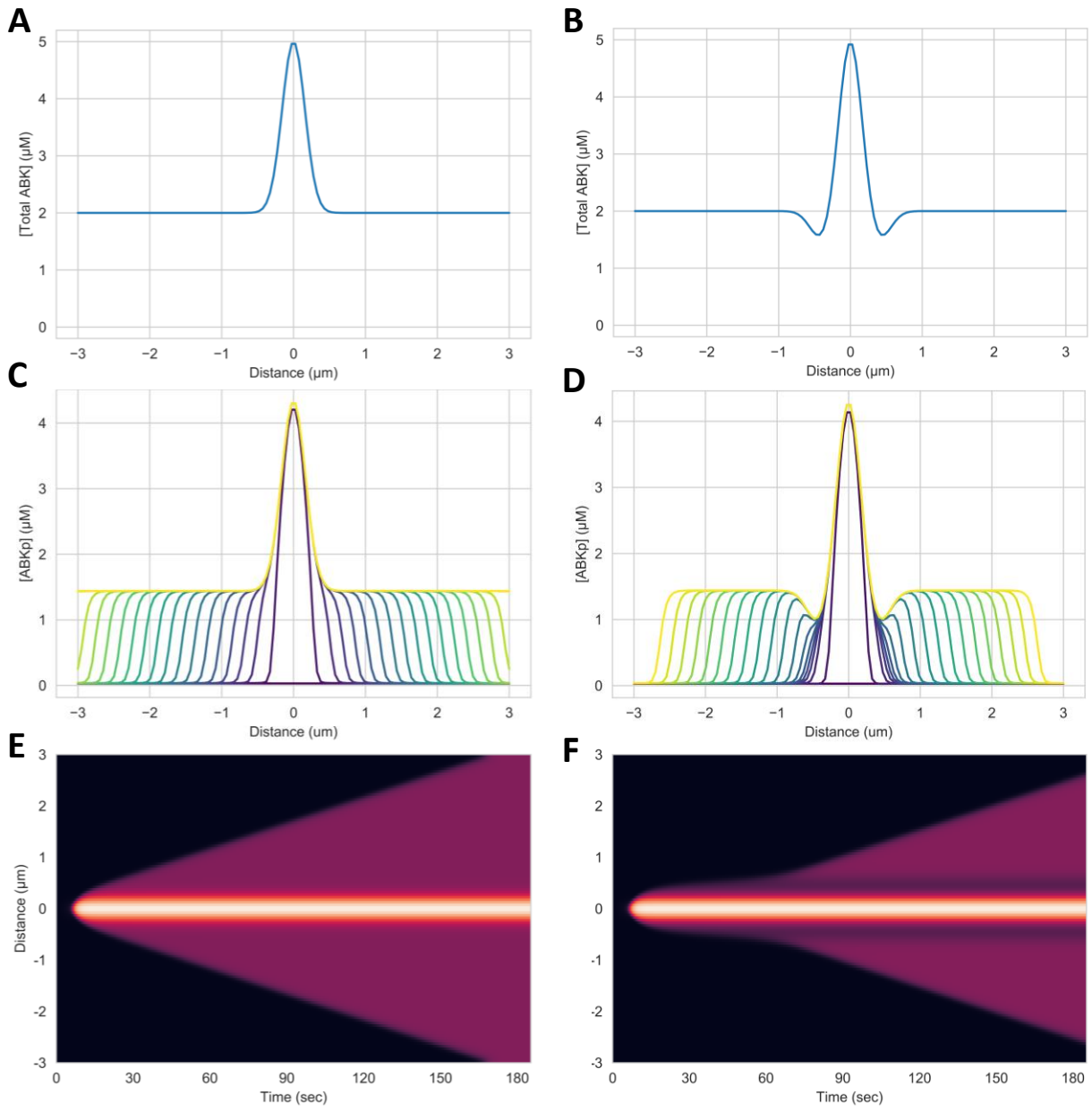

Figure 16: Traveling Fronts in the Phenomenological Model. (A) Total Aurora B kinase profiles without kinase valleys (B) and with valleys. (C/D) Corresponding spatial profiles using 0.65 μM phosphatase and D = 1E-3 μm²/s. (E/F) Corresponding heatmaps.

directly by passing activated kinase across the valley. Faster reaction speed will be able to cross the region without stalling. Situations with either slower reaction speed or slower diffusion will be pinned and not be able to cross this region.

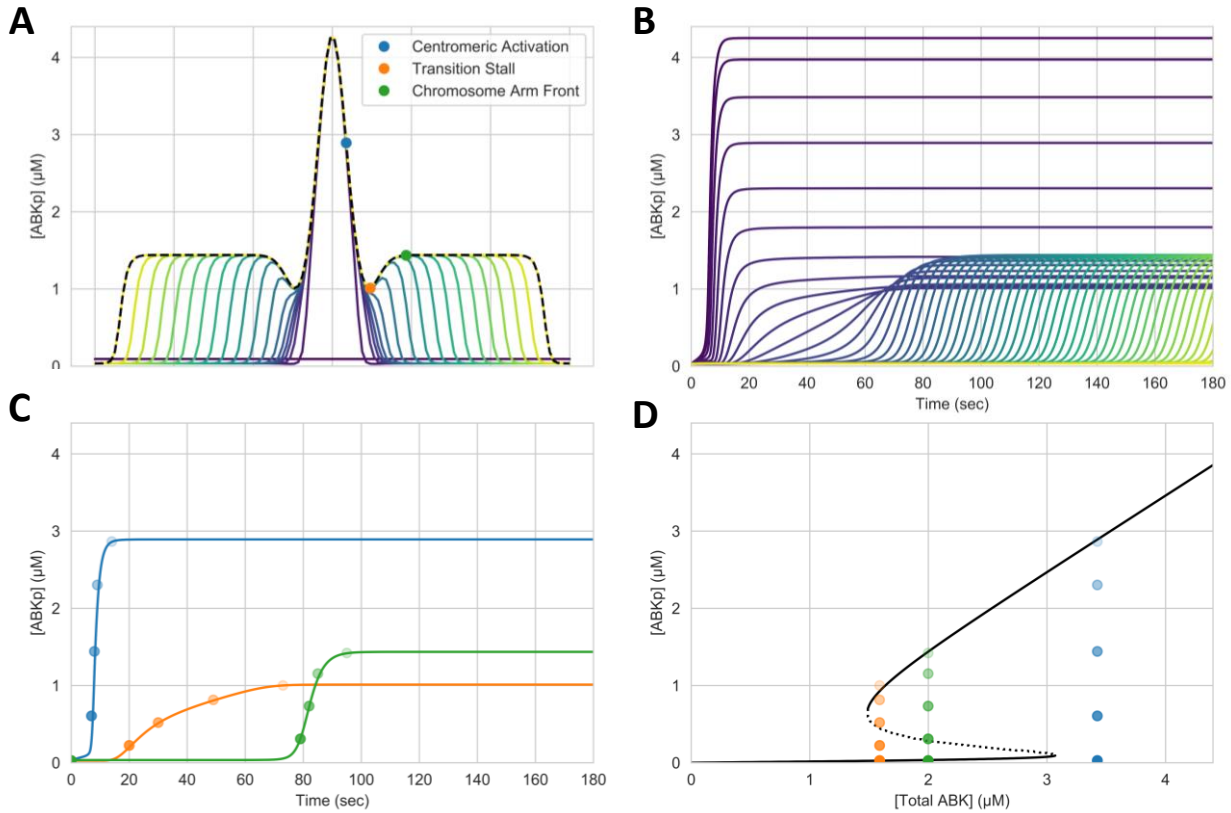

Figure 17: Three Regions in Traveling Front Propagation. (A) Spatial profile highlighting representative points for the three regions. Same conditions used as Figure 16B/D/F. (B) Temporal profile with each line corresponding to individual spatial slices. (C) Three chosen representative spatial slices with four time points in decreasing transparency chosen per spatial slice. Time points chosen in relation to 20, 50, 80, and 99 percent activation with respect to the high steady state. (D) Four time points of the three spatial slices plotted related to the bistability curve.

The stalled front situation can be broken into three regions: centromeric activation, traveling front propagation along the arms, and the transition period between the two. The regions are illustrated by the blue, green, and orange points, respectively, in Figure 17A. By looking at the system as the spatial progression of a temporal profile, rather than the temporal progression of a spatial profile, behavior across time in each region can be seen more clearly (Figure 17B). Three spatial slices representative of the three regions can be used to describe the dynamics with respect to the bistability curve (Figure 17C/D). Since phosphatase concentration is a constant in our simplified model, the bistability curve with respect to total kinase concentration is constant in time. The three spatial slices with their activated kinase concentrations are plotted with time corresponding to the decreasing transparency of the plotted points. It can be easily seen that the centromeric activation region is in the monostable region dominated by the activated branch, thus these points autoactivate with no perturbation necessary. The transition region is the farthest left in the bistability curve and has to cross a higher threshold than the points along the chromosome arms, therefore activation time is longer. Moving past the kinase valley onto the chromosome arm, the final region regains front travel speed and its sigmoidal shape as the bistability threshold decreases. A movie of this process in the Supplemental section can more clearly show this process the limits of spatiotemporal discretization (Supplemental Movie 1).

6.6. Geometric Analysis & the Maxwell Point in the Phenomenological Model

A different approach must be used to explain the transient approach to an energetic equilibrium seen in the stalling behavior around the kinase valleys. A derivation of speed and directionality of traveling front propagation can be useful[39,43]. The result from previous work is reproduced in the following equation:

$$c = \frac{\int_{lo\_ss}^{hi\_ss} r(A)dA}{\int_{-\infty}^{\infty} \left(\frac{dA}{dz}\right)^2 dz}$$

where c is front travel speed, hi_ss is the point at which $r(A) = 0$ and $r'(A) = -1$ and thus corresponds to the high steady state activated kinase concentration, lo_ss corresponds to the low steady state, and z is a spatial variable used in the analysis where $z = x - ct$.

Since the denominator in the expression for front speed is always positive, front direction is determined solely by the numerator[39,43]. Therefore we can establish the fate of bistable traveling fronts by comparing the areas above and below the x-axis of the net activation rate with respect to active kinase concentration, bounded by the low and high steady states. If the system is monostable, the high and low steady states coalesce and a traveling front solution technically does not exist, although there will be movement towards the monostable point with a direction corresponding to whether the curve is above or below the x-axis.

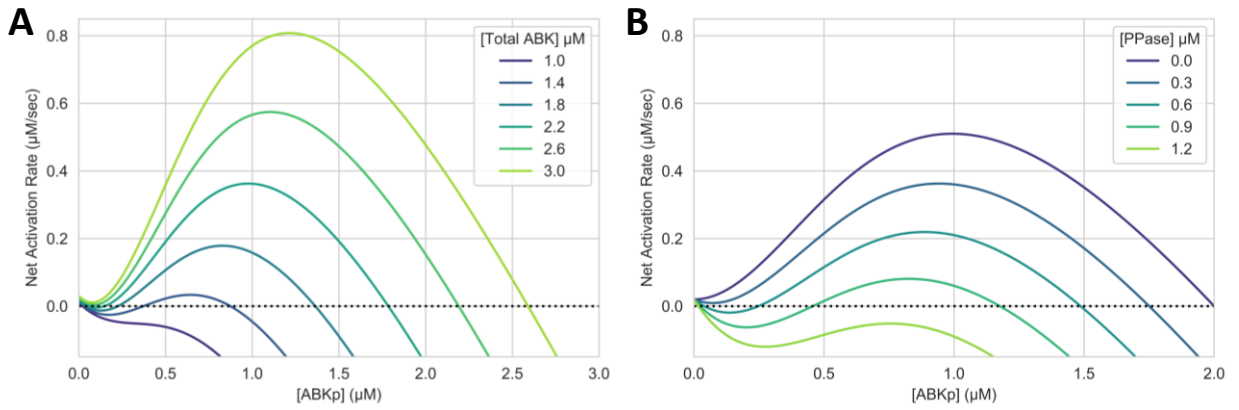

Figure 18: Geometric Analysis. (A) Activation rate curves with differing total kinase concentrations (B) and differing phosphatase concentrations. The net area between the curve and the x-axis dictates the direction of a traveling front.

Geometric analysis can thus be performed by plotting activation rate with respect to activated kinase and varying either total kinase or phosphatase concentration (Figure 18). At high total kinase or low phosphatase concentrations, the activation rate curve crosses the x-axis only at high active kinase concentrations, therefore the system has a monostable active steady state as we see in the centromeric activation region. Decreasing total kinase or increasing phosphatase, the activation curve eventually crosses the x-axis in three points. The low and high points are steady states while the middle point is the bistability threshold. The system thus gains bistability, initially with an area above the x-axis greater than below, which describes an activating front as we see along the chromosome arms. At lower total kinase or greater phosphatase, the relative areas shift to favor the area below the x-axis and the activating front gradually slows to a stop and then flips to an inactivating front. The transition from activating to

inactivating front, the Maxwell point, are where the forces behind activating and inactivating fronts are equal and a traveling front stops, illustrated graphically by equal areas above and below the x-axis[21,41].

With this geometric based analysis, behavior at the stall transition region can be visualized (Figure 19A). The entire area is above the x-axis at the centromeric region. At the transition region, the area below in fact is slightly greater than above, yet diffusion across the kinase valley overcomes this 'sink' effect of the local inactivation force. As the front pulls out into the chromosomal arms, the activation force once again dominates.

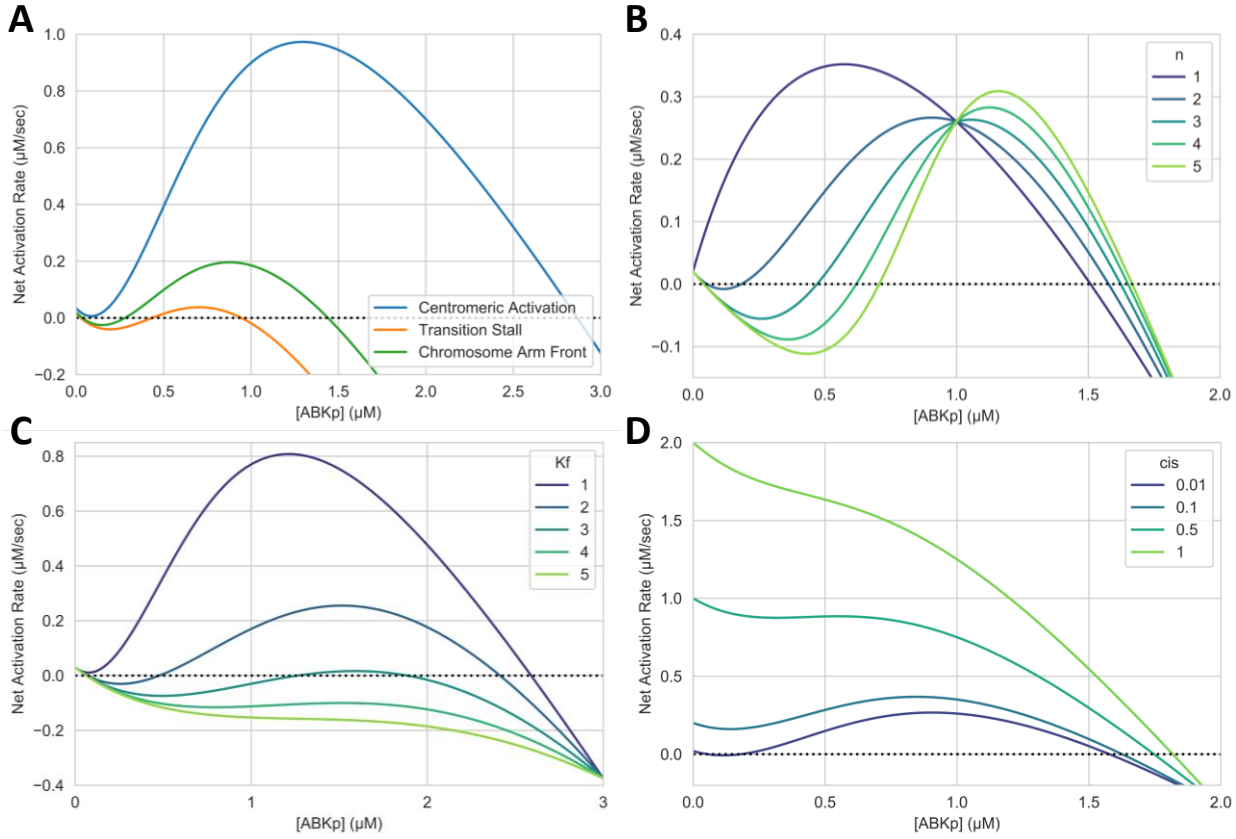

Figure 19: Using geometric analysis to describe: (A) the stalling behavior in the transition region, (B) vanishing bistability as activation loses its nonlinearity, (C) vanishing bistability as in trans complexing decreases stability, (D) vanishing bistability as activation loses its nonlinearity relative to in cis activation. (A) uses the same conditions as in Figure 16B/D/F with total kinase corresponding to the three spatial points, (B/D) uses 2 uM total kinase and 0.5 uM phosphatase, (C) and uses 3 uM total kinase and 0.5 uM phosphatase)

Additional insight can be gathered using this means of visualizing bistability while changing various parameters in the model (Figures 19B/C/D). Bistability vanishes with an activation Hill coefficient lower than one, high K_f, or high k_{cis}. The first reiterates intuition shown earlier, that cooperativity or nonlinearity in activation is required for bistability. The second indicates the need for stable in trans complexing of inactive and active kinase, as described by low K_f or high binding rate relative to unbinding or reaction rates. And the last shows that as the reaction rate of the in cis pathway is increased relative to in trans, effective nonlinearity is reduced in relation to the in trans pathway and bistability disappears. Though reducing in cis activation to zero pulls the entire first part of the curve below the x-axis and would eliminate any possible centromeric autoactivation. There is therefore a

bounded window for the in cis reaction rate that allows this model to demonstrate centromeric activation and a chromosomal bistable traveling front.

Using logic gained from this geometric analyais, a pinned front can be demonstrated by approaching the Maxwell point with a gradually decreasing total kinase slope along the chromosome arms (Figure 20). Instead of slowing down as in the kinase valleys of the transition region, the front propagation stops at the Maxwell point in the outer arm.

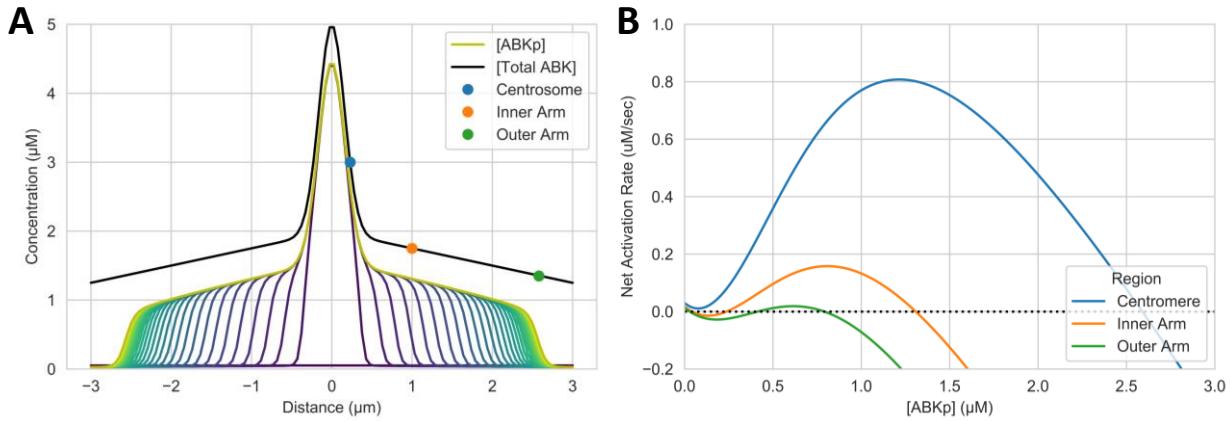

Figure 20: Pinned Wave. (A) Total kinase profile and resulting activation traveling front with three representative spatial slices chosen and (B) its corresponding net activation curves, showing the front stopped at the Maxwell point in the outer arm. Simulations used 0.5 uM phosphatase.

6.7. Dynamic Kinase & Phosphatase in the Mass-Action Model

Moving back to the mass-action model, the picture gains a few dimensions. The total kinase profile is dynamic in time as well as space, and phosphatase can diffuse towards its substrate, active kinase. Thus, the bistability curve moves left or right according to local phosphatase concentration. And the local kinase concentration determines the x-coordinate relative to this dynamic bistability curve. The changing shape of a bistability curve due to spatial relocalization has been shown in a recently published paper to provide extra control over the timing and robustness of cell cycle transitions[44].

These dynamic interactions build an interrelated system in which the kinase responds to the binding sites and activates according to local kinase and phosphatase concentrations. The phosphatase then responds to the activated kinase, in turn affecting the activation rate of local inactive kinase. A seven panel movie in the supplemental section (Supplemental Movie 2) illustrates the spatiotemporal dynamics of the bistability curve with respect to activated kinase, total kinase and phosphatase concentrations at three representative spatial slices. Static depictions of the evolution of these key parameters in space and time are demonstrated in Figure 21. However bistability curve dynamics have not been reproduced in static form given the movie much more adequately shows the behavior.

Although kinase is initially evenly distributed, diffusion towards binding sites quickly reproduces a profile similar to that used in the phenomenological model, centromeric dominant with a surrounding valley emerging at sufficiently low diffusion speeds. Increasing kinase in the centromere pushes the system out towards the monostable active branch of the bistability curve, stimulating autoactivation. Phosphatase then binds to the activated kinase, pulling in nearby free phosphatase and pushing the bistability curve to the right. However this does not affect activation speed in the inner centromere since the activated kinase population has already sufficiently passed the bistability threshold.

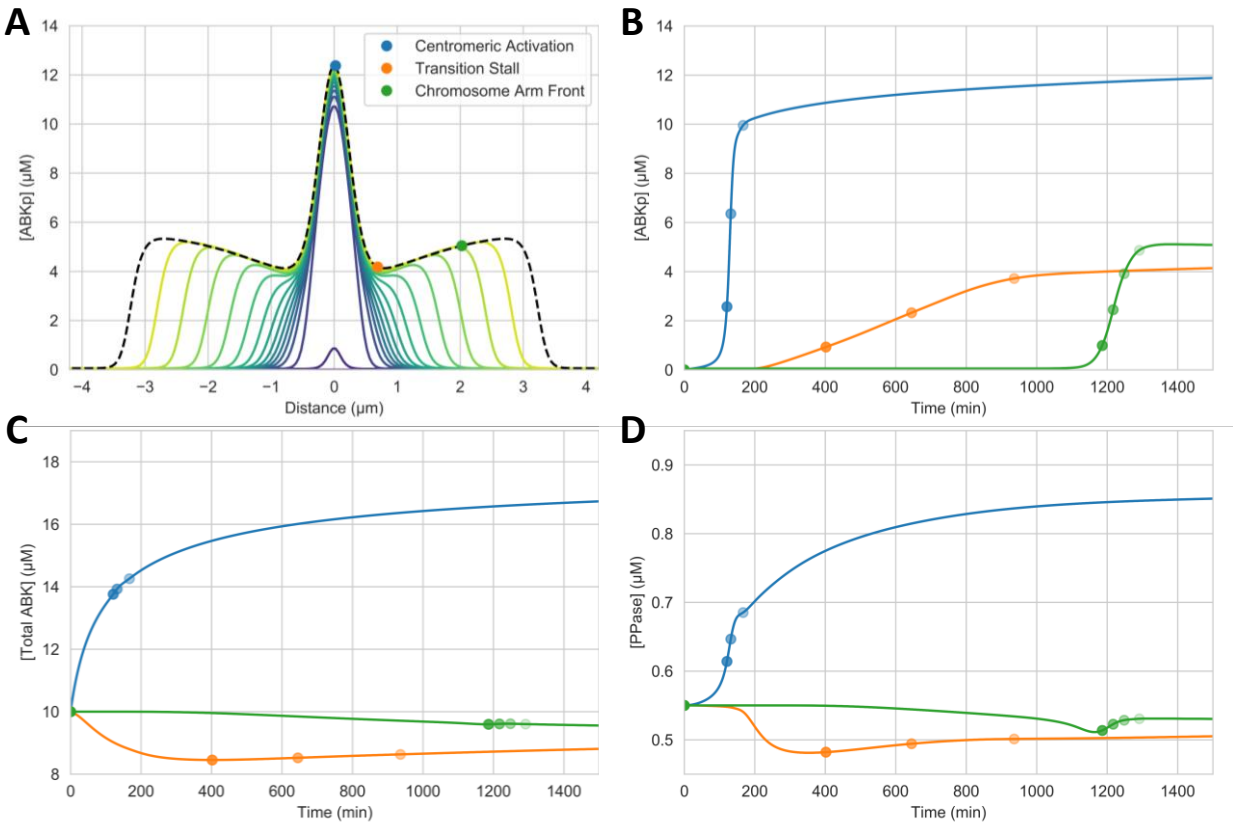

Figure 21: Kinase & Phosphatase Dynamics in the Mass-Action Model. (A) Spatial activation traveling front with three representative spatial slices and corresponding temporal representations of (B) activated kinase, (C) total kinase, and (D) phosphatase. Time points chosen in relation to 20, 50, 80, and 99 percent activation with respect to the high steady state. Simulations were run with 0.55 μM phosphatase, 10 μM total kinase, and D = 1E-5 μm²/s.

Meanwhile, the surrounding points experience counterbalancing effects in local concentrations of both kinase and phosphatase with respect to the inner centromere. The kinase valley resulting from diffusion towards centromeric binding sites pulls the system to the left and into the monostable inactive branch of the bistability curve. The phosphatase movement towards activating centromeric kinase generates a parallel valley in phosphatase, pushing the bistability curve to the left, such that the system is back in the bistability region. Diffusion of activated kinase from the centromere slowly pulls local active kinase concentration above the bistability threshold and towards the active branch of the curve.

The chromosome arms do not experience substantial kinase or phosphatase dynamics due to the lack of spatial heterogeneity in the surrounding binding site profile. Although, local phosphatase concentration marginally decreases just before the traveling front reaches a particular point due to diffusion towards the oncoming active kinase front. This triggers a faster activation due to a shift left in the bistability curve and a corresponding decreasing threshold. In combination with the relatively unchanging kinase concentration, this increases front travel speed.

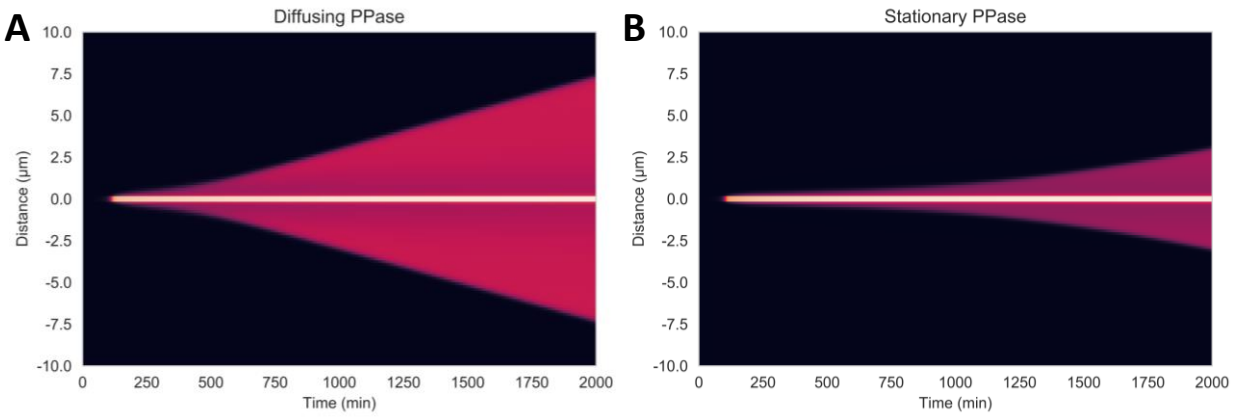

Figure 22: Effect of Phosphatase Dynamics. (A) Heatmap of Aurora B activation with diffusible phosphatase (B) and with fixed phosphatase. Simulations were run with the same conditions as in Figure 21 although with a narrower binding site profile.

As a loss-of-function mutation can elucidate the role a certain gene or protein may play in a network, phosphatase movement can be restricted to observe its effect on front propagation. As before, diffusing kinase leads to centromeric autoactivation and a surrounding kinase valley. The lack of phosphatase diffusion, however, prevents the bistability curve from shifting left and speeding up activation along the chromosome arms. The threshold therefore maintains a higher barrier relative to the diffusing phosphatase situation. This increases the length of the stall in the transition region as well as decreases front propagation speed along the arms, seen in Figure 22 as well as in the more comprehensive demonstration in Supplemental Figure 18. In situations where the minimum local kinase concentration pushes the region to the left of the bistability region and onto the monostable inactive branch, the front does not progress into the arms and stays pinned to the centromere (Supplemental Figure 19). Therefore, as has been previously shown, spatiotemporally dynamic components in a bistable system can greatly affect transition timing and speed[44].

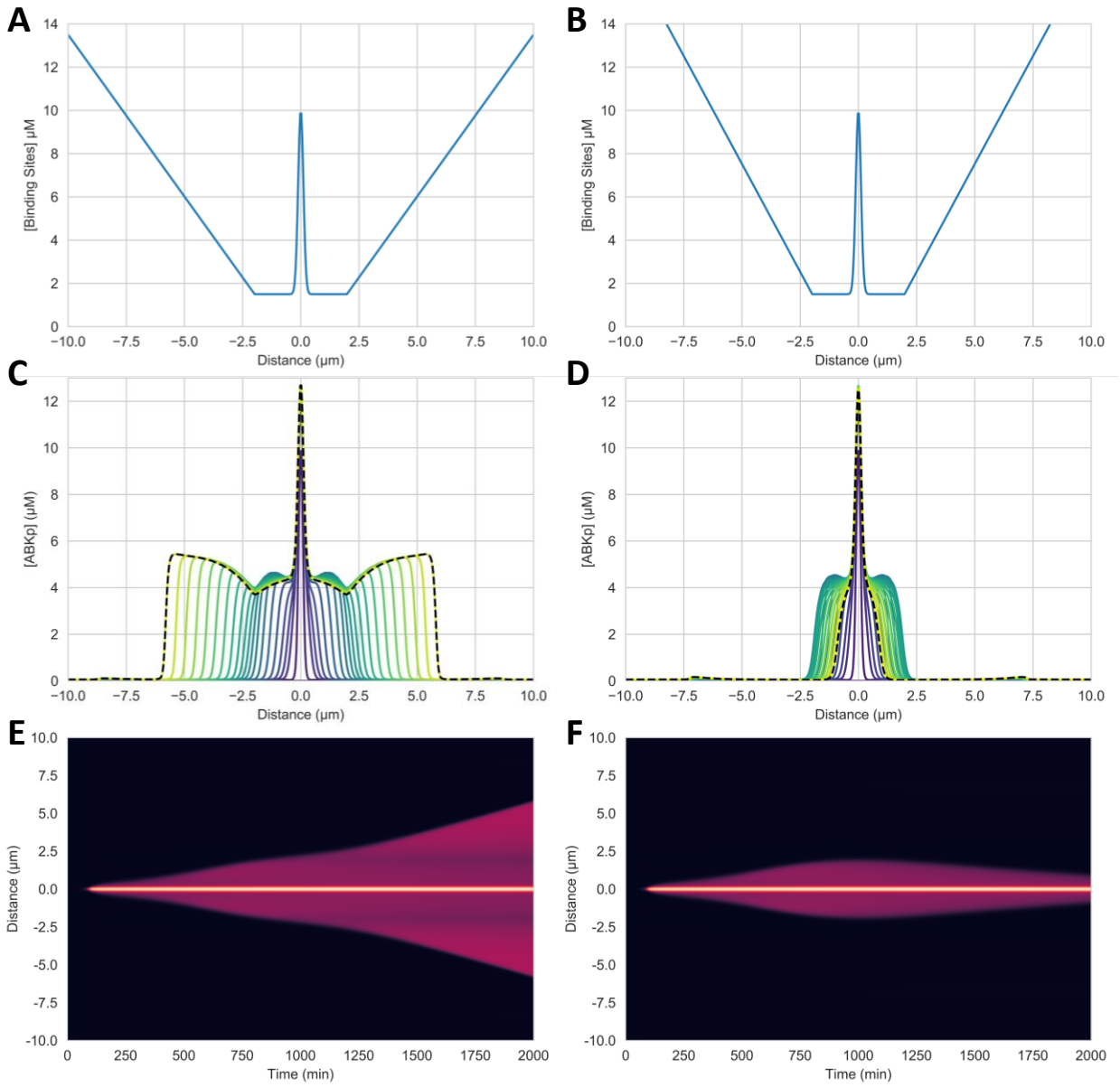

Figure 23: Binding Site Profiles with Ramps. (A) Binding site profiles with ramps along chromosome arms at slopes of 0.25 µm (B) and 0.33 µm per spatial interval, of which there were 120 across the 20 µm simulated length. (C/D) Corresponding spatial profiles evolving in time. (E/F) Corresponding heatmaps.

Altering the binding site profile can lead to interesting behaviors, such as introducing a second stall and a dynamic front reversal. Given that a kinase valley can stall or stop a traveling front, a particular pattern of binding sites can coordinate kinase movement by building a suitably steep valley outside the boundary of the centromere. This can simply be done by adding a linear ramp of binding sites on either side of the centromere (Figure 23). Diffusion towards the higher binding site concentration gradually shifts kinase from the bottom of the ramp towards the top, forming a valley at the ramp base. With intermediate binding site ramp slopes and shallower kinase valleys, this manifests as a second stall as the front slowly crosses the valley. At higher slopes, the kinase valley is enough to stop the front and continues deepening over time, pushing the front back towards its original centromeric boundary. A dynamic

illustration has been generated as a movie in the supplemental section (Supplemental Movie 3) as well as a discretized version (Supplemental Figure 20).

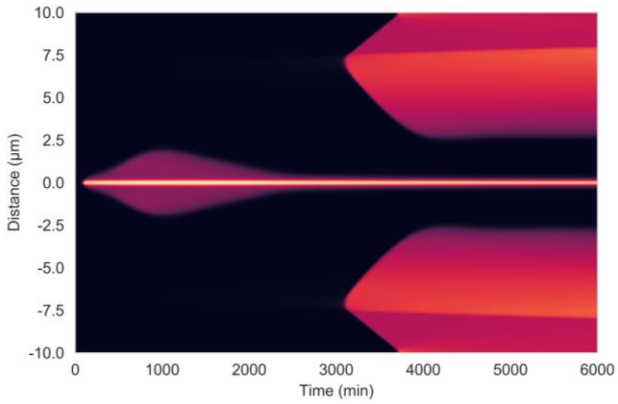

Figure 24: Long term evolution of kinase activation with a binding site ramp of 0.33 μm per spatial interval and its development of a long-term stable pattern.

Continuing the simulation of such systems leads to another interesting phenomenon, autoactivation in non-centromeric regions. This is especially evident in the system with the higher ramp slope given the reversal of its initial centromeric front (Figure 24). As kinase moves toward binding sites farther along the chromosome arms and towards the denser concentration of binding sites, kinase eventually crosses the hysteretic threshold to the autoactivating monostable branch.

A curious point is that the traveling front that follows the autoactivation in the outer arms travels in a similar speed in both directions despite the difference in kinase concentration. As time progresses, the kinase profile gradually shifts to reflect the binding site profile, moving from the centromere outwards. This behavior and its consequences are perhaps best illustrated as a movie (Supplemental Movie 4), although the time evolution of spatial profiles are included as Supplemental Figure 21. At the points of autoactivation, there is a distinct asymmetry in kinase on either side, greater on the inward side than the outward. As we have seen earlier, lower kinase concentration is farther left on the bistability curve, corresponding to a greater threshold and slower activation speed all else equal. Yet local phosphatase concentration is not equal. Due to the kinase asymmetry, autoactivation occurs asymmetrically, with a sharper slope on the outward side with less kinase. This prompts a sharper response in phosphatase diffusion from the outward side, thus a deeper phosphatase well proximal to the activating front. This appears to nullify the effect from the lower kinase by pushing the bistability curve left, lowering the threshold, and quickening outward front travel speed. This analysis however has not been fully developed and is an open question, yet can be theoretically postulated given previously developed intuition.

Another point of interest is the long-term stability of the system after the inwardly traveling front approaches its Maxwell point at the deep kinase wells in the centromeric proximal region. Here the fronts slow to a halt and are pinned, where activation and inactivation forces balance. In this way, it is possible to imagine that one can construct transiently dynamic, long-term stable patterns in this manner. Sharp spikes of binding sites could be used to quickly attract surrounding kinase to autoactivate and begin the initial outward traveling fronts. Broad peaks of binding sites develop equally broad ramps of kinase that have potential to pin and reverse oncoming traveling fronts. At a later point, the peaks amass enough kinase to autoactivate and start their own traveling fronts that meet kinase wells built by the spikes. This was not tested to an extent to present in this report but harnessing the combined powers of reaction, diffusion, and localization to create such patterns could be a direction of further study.

7. Conclusions

At the start of this thesis, the goal had been to reproduce the spatial Aurora B activity gradient responsible for controlling chromosome separation in mitosis. As outlined in the previous sections, the project has experienced two major changes of direction, ultimately leading to an unexpected exploration in a unique space of the combination of bistable reaction, diffusion, and localization forces.

In the first section of the results, we learned the underpinnings of bistability. Balancing both positive and negative feedback loops in Aurora B activation is needed to reproduce bistability within the system. The nonlinear phenomenon imparts history-dependence, critical thresholding via inhibitor ultrasensitivity, and a type of noise filter via hysteresis. Furthermore the two key models, mass-action and phenomenological, were introduced allowing exploration of both the complicated multilayer dynamics of the full system as well as the analytical ease of the simplified system.

In the next section, the beginning portion of the reconstruction of a minimal kinase-phosphatase system was discussed, both in principle and in results. The essence of such a system lies within the activation portion of Aurora B kinase and the necessary activating INbox of INCENP. The two proteins genetically encoded on plasmid vectors were amplified, sequenced, transformed, and expressed. However purification of the Aurora B-INbox complex was not successful, likely due to protein aggregation with several potential root causes. Plasmid material, protocols, and data have been kept for future potential work.

In the last section, we explore the spatial aspects of simulating the kinase-phosphatase system by asking a series of questions, alternating between the two models as needed. The combination of bistable reaction kinetics and diffusion can result in traveling fronts, where a constant travel speed and amplitude can be achieved across space and time. Localization of couples with diffusion to create the spatial origin of the kinase activity gradient.

While simulation of activation dynamics in the Aurora B kinase-phosphatase system has been shown to reproduce the constant speed and amplitude of a bistable traveling front, the length scale of a front is significantly greater than the relevant chromosomal length. In other words, the spatial gradient created from a bistable traveling front is flat along the length scale of a chromosome rather than having the experimentally observed sharply-defined boundaries. This is then shown to be due to a much greater diffusion speed relative to activation, causing a shallow gradient or collapse in the bistable region. This leads to the conclusion that a bistable traveling front, using the parameters and structure of the mass-action model described, cannot produce a spatial activity gradient seen experimentally or published in the paper by Zaytsev et al.

It cannot be known for sure what error Zaytsev et al had made in their claim, without knowing exactly how they set up their simulations. Given that it was possible to reproduce their reaction kinetics, the disconnect was likely not there. There may be an issue with how the spatial aspects, such as accidentally using a higher diffusion speed due to a unit conversion mistake, quite possible in the simulation space. It could be that they were using a different parameter set or different initial conditions, and that the activation front they simulated was not a bistable traveling front. Given the high dimensionality of this system, it is a nontrivial task to fully probe the system for how they setup their calculations.

Instead of looking into experimentally realistic simulation, the direction chosen at this point was to observe traveling front behavior with reduced diffusion speed. This allowed an interesting spatially

heterogeneous phenomenon involving centromeric autoactivation and emergent traveling fronts outward along the chromosome arms. At certain ranges of parameters, a stalling behavior in the transition region between the centromere and chromosome arms was observed. The phenomenological model was used to explain how these different regions passed distinct portions of the bistability curve due to kinase diffusion. And geometric analysis was employed by examining the area between the net activation curve and the x-axis, which described the transition region as passing by a Maxwell point where reaction forces are equalized.

The intuition gained in the simplified model was taken back to the mass-action model to explain behavior with dynamic kinase and phosphatase concentrations. Here we find kinase responding to the binding profile, autoactivating once reaching the monostable threshold, and phosphatase responding to the activated kinase. While decreasing centromeric-proximal kinase slows down or stops a potential traveling front, decreasing phosphatase in response to activating centromeric kinase reverses this effect. Along the chromosome arms, these dynamics are not as prominent yet locally diffusing phosphatase towards an oncoming traveling front quickens its propagation speed. Also briefly explored, binding site ramps along chromosome arms instill second order kinase dynamics, where secondary kinase valleys can produce a second stalling period or can even reverse a front. On a greater time scale, the kinase can push the local system into the autoactivating region and initiate its own traveling fronts which develop into an interesting long-term stable means of pattern formation.

8. Outlook

As the unexpected result was approached, that traveling fronts were not relevant on the length scale of a chromosome, two paths diverged. On the one hand, the model could be altered to attain better experimental relevance either by including new aspects or by losing the demand to look for bistable traveling fronts. On the other hand, the diffusion speed could be reduced such that bistable reaction, diffusion, and localization forces were balanced and interesting spatial phenomena could be explored. While the latter was chosen, the possibilities of the former will be discussed.

First of all, the finding that bistable fronts were too wide to be relevant for chromosome simply invalidates fronts as relevant in the system as described by the mass-action model formed by Zaytsev et al. Traveling fronts may still be the underlying cause of the sharply defined spatial activity gradient in mitosis. But given the complexity of the interaction network of Aurora B and the CPC, it is quite likely that other interactions not described in the mass-action model, such as interactions with microtubules, are relevant to the spatial behavior of Aurora B[6,11,12]. INCENP, Survivin, and Borealin each have localization properties that may affect the dynamics, effectively slowing down the diffusion speed of the CPC enough that traveling front becomes relevant[11]. The diffusion speed for the CPC used in this model was calculated using the Stokes radius, which does not account for other factors that could affect the speed of diffusion[10]. Furthermore, both phosphatase targeting and regulation by Aurora B have been cited before as contributing to the dynamics in the system and were not factored into the Zaytsev model[45,46].

Another route could be to fit experimental behavior to the model parameters and initial condition of the Zaytsev model in order to find how they ran their simulations. This could entail a 'sweep' of the parameter space, that includes regions of the parameters not considered in this project.

As for extending the explorations found using a reduced diffusion speed, there is the clear limitation that these simulations used a significantly lower diffusion speed than had been calculated. While being of questionable direct significance to the Aurora B kinase-phosphatase system, the theoretical underpinnings of the intuition gathered for this unique system of bistable reaction, diffusion, and localization could be used in many other areas, such as liquid crystals or population dynamics[36,37].

First, further work could be done by defining parameter ranges in which one can observe the various behavior outlined in the report. These behaviors include centromeric activation, traveling fronts along the chromosomal arms, stalling transition regions, pinned waves, reversed waves, etc. It would be of great visualization value to construct sweep maps that outline the boundaries in a two dimensional format. Although given the high dimensionality of the system, reducing the system to two parameters would have its limitations. Reviewing the effect of binding site profiles would be difficult in this format.

Work on the simplified system can be extended to include localization forces. A recent comprehensive review discusses a geometric-based approach to analyzing a two component system with different diffusivities[47]. The intuitive nature of such an approach is extremely appealing, and it explains the front pinning behavior of cell polarization[39]. However localization to binding sites is a higher dimension, requiring at least two inactive components and two active components for bound and unbound designations. It is not clear if such a system can be sufficiently simplified in a similar way to Brauns et al, where the reactive, diffusive, and localizing forces and phase spaces can be decoupled and geometrically related.

The spatial aspects could be extended to higher order binding site patterns or to higher dimensions to observe more complex phenomenon. By utilizing the directive power of binding sites, unique mixtures of transient and long-term pattern formation could be achieved. While this is conceptually interesting, perhaps this could have some future experimental potential as well. The study of combined reaction and diffusion has been studied for decades now, yet the combination of localization does not seem to be well explored. This is curious given how the addition of binding to a reaction-diffusion system seems like relatively simple to implement. The explorations in this thesis appear to have approached a space that has not been developed, where a traveling front is pinned or momentarily stalled due to a dynamically changing input. Higher dimensions could be added to this system as well to spatially extend the system in order to create patterns such as dots or stripes. In addition, phosphatase localization or additional regulation could be included to further extend the complexities and potential behavior of the system.

Furthermore, source and degradation terms could be included in the reaction kinetics to create localized patterns via subcritical Turing bifurcations and homoclinic snaking[48]. These terms would break the limits of material conservation and allow for more complex nonlinear behavior. Although while theoretically interesting, it remains to be seen how this research direction would be experimentally significant.

9. Methods

9.1. Theoretical

All simulations were coded in Python. The system of ordinary differential equations (ODEs) describing temporal simulations of the well-mixed, non-spatial system were solved using the built-in scipy.integrate.odeint. The mass-action ODE system used involves the following equations:

$$\frac{dA}{dt} = \left(k_{cis} - k_f^a * A\right) * a + (k_r^a + 2k_c^a) * [Aa] - k_f^p * A * P + k_r^p * [PA]$$

$$\frac{d[Aa]}{dt} = k_f^a * A * a - (k_r^a + k_c^a) * [Aa]$$

$$\frac{dP}{dt} = -k_f^p * A * P + \left(k_r^p + k_c^p\right) * [PA]$$

$$a = A_{tot} - A - 2[Aa] - [PA]$$

$$[PA] = P_{tot} - P$$

Partial differential equations (PDEs) describing spatiotemporal simulations of the spatially heterogeneous systems were solved using a constructed algorithm containing forward differencing for the time derivative and a spectral method for the space derivative. The specific spectral method used was a Fourier mesh, which was about twenty times faster than central difference and twelve times faster than the built-in scipy.fft. Boundary conditions used for the space derivatives were periodic as a result of using a spectral method. It can be demonstrated that there is minimal difference from zero flux, or Neumann, and periodic boundary conditions due to the symmetric spatial profiles involved (Supplemental Figure 22).

Without kinase localization, the mass-action PDE system involves:

$$\frac{\delta a}{\delta t} = -\left(k_{cis} + k_f^a * A\right) * a + k_r^a * [Aa] + k_c^p * [PA] + D\frac{\delta^2 a}{\delta x^2}$$

$$\frac{\delta A}{\delta t} = \left(k_{cis} - k_f^a * A\right) * a + (k_r^a + 2k_c^a) * [Aa] - k_f^p * A * P + k_r^p * [PA] + D\frac{\delta^2 A}{\delta x^2}$$

$$\frac{\delta [Aa]}{\delta t} = k_f^a * A * a - (k_r^a + k_c^a) * [Aa] + D\frac{\delta^2 [Aa]}{\delta x^2}$$

$$\frac{\delta P}{\delta t} = -k_f^p * A * P + \left(k_r^p + k_c^p\right) * [PA] + D\frac{\delta^2 P}{\delta x^2}$$

$$\frac{\delta [PA]}{\delta t} = k_f^p * A * P - \left(k_r^p + k_c^p\right) * [PA] + D\frac{\delta^2 [PA]}{\delta x^2}$$

With kinase localization, the mass-action PDE system adds in B for activate, bound kinase and b for inactive, bound kinase:

$$\frac{\delta a}{\delta t} = -\left(k_{cis} + k_f^a * A + k_f^a * B\right) * a + k_r^a * ([Aa] + [Ba]) + k_c^p * [PA] + k_{off} * b - k_{on} * BS * a + D\frac{\delta^2 a}{\delta x^2}$$

$$\frac{\delta b}{\delta t} = -\left(k_{cis} + k_f^b * A + k_f^b * B\right) * b + k_r^b * [Bb] + k_r^a * [Ab] + k_c^p * [PB] - k_{off} * b + k_{on} * BS * a$$

$$\frac{\delta A}{\delta t} = \left(k_{cis} - k_f^a * A\right) * a + (k_r^a + 2k_c^a) * [Aa] - k_f^p * A * P + k_r^p * [PA] + k_c^a * [Ba] - k_f^a * A * b + (k_r^a + k_c^a) * [Ab] + k_{off} * B - k_{on} * BS * B + D\frac{\delta^2 A}{\delta x^2}$$

$$\frac{\delta B}{\delta t} = \left(k_{cis} - k_f^b * B\right) * b + \left(k_r^b + 2k_c^a\right) * [Bb] - k_f^p * B * P + k_r^p * [PB] + k_c^a * [Ab] - k_f^a * B * a + (k_r^a + k_c^a) * [Ba] - k_{off} * B + k_{on} * BS * B$$

$$\frac{\delta [Aa]}{\delta t} = k_f^a * A * a - (k_r^a + k_c^a) * [Aa] + D\frac{\delta^2 [Aa]}{\delta x^2}$$

$$\frac{\delta [Ba]}{\delta t} = k_f^a * B * a - (k_r^a + k_c^a) * [Ba]$$

$$\frac{\delta [Ab]}{\delta t} = k_f^a * A * b - (k_r^a + k_c^a) * [Ab]$$

$$\frac{\delta [Bb]}{\delta t} = k_f^b * B * b - (k_r^a + k_c^a) * [Bb]$$

$$\frac{\delta P}{\delta t} = -k_f^p * (A + B) * P + \left(k_r^p + k_c^p\right) * ([PA] + [PB]) + D\frac{\delta^2 P}{\delta x^2}$$

$$\frac{\delta [PA]}{\delta t} = k_f^p * A * P - \left(k_r^p + k_c^p\right) * [PA] + D\frac{\delta^2 [PA]}{\delta x^2}$$

$$\frac{\delta [PB]}{\delta t} = k_f^p * B * P - \left(k_r^p + k_c^p\right) * [PB]$$

$$BS = BS_{tot} - B - b - [Ba] - [Ab] - 2[Bb] - [PB]$$

Parameters used in the mass-action model were as follows:

PARAMETER	*VALUE*	*UNITS*
$\boldsymbol{k_{cis}}$	7.29 x 10^{-6}	s^{-1}
$\boldsymbol{k_f^a}$	0.1	$uM^{-1}s^{-1}$
$\boldsymbol{k_f^b}$	$k_f^a * 0.01 = 0.001$	$uM^{-1}s^{-1}$
$\boldsymbol{k_r^a}$	5.073	s^{-1}
$\boldsymbol{k_r^b}$	0.024	s^{-1}
$\boldsymbol{k_c^a}$	2.7 x 10^{-2}	s^{-1}
$\boldsymbol{k_f^p}$	0.6	$uM^{-1}s^{-1}$
$\boldsymbol{k_r^p}$	1.146	s^{-1}
$\boldsymbol{k_c^p}$	2.4 x 10^{-2}	s^{-1}

k_{on}	2.9	$uM^{-1}s^{-1}$
k_{off}	0.014	s^{-1}

9.2. Experimental

Amplification & Sequencing

Two pGEX-6P-2 plasmids modified with DNA sequences for Aurora B and INCENP were amplified in E. coli DH5α cells. One contained Aurora B^{45-344} and $INCENP^{790-856}$ of Xenopus laevis, courtesy of the Grishchuk lab. The other contained Aurora B^{FL} and $INCENP^{835-903}$ of Homo sapiens, courtesy of the Aleyde lab. The N-terminal domain of Aurora B has been reported to not affect kinase activity or INCENP binding[18]. As for INCENP, only the minimal domain required for Aurora B binding and activation, called the INbox was included[18]. The plasmids were constructed such that the Aurora B would be expressed as a fusion protein with a GST tag, cleavable via a PreScission cut site, and the INCENP fragment would be expressed as a separate protein with its own ribosome binding site[26]. The tac promoter for both constructs were regulated by a lac operator, thus their expression was inducible only in the presence of IPTG[26]. Amipicillin resistance was also added so as to allow only successfully transformed colonies to grow in a medium containing ampicillin[26].

After unfreezing the E. coli cells, courtesy of the Aleyde lab, the plasmid was added and transformed via a heat shock of 45 sec in a water bath kept at 42°C. Medium (lysogeny broth) was then added to this mixture and the tube was shaken for an hour before spreading on a plate containing medium, agar, and ampicillin and incubated overnight at 37°C. To amplify successfully transformed bacteria, colonies were picked from the incubated plate and used to inoculate tubes of medium with ampicillin, which were then incubated overnight.

The amplified plasmid was then extracted using an EZLA DNA Mini Kit. A NanoDrop was used to quantify DNA concentration. The DNA was then sent out to LGC Genomics for Sanger sequencing. Using the received data, I aligned the sequences with known sequences of unmodified pGEX-6P-2 plasmid to confirm the protein sequences used in each plasmid.

Transformation & Expression

The plasmids were transformed in E. coli BL21(DE3)pLYS cells using the same heat shock procedure as described above. Instead of picking individual colonies, the entire plate is wiped for inoculation into a tube of medium and ampicillin. After overnight incubation, the tube is then transferred to a flask with a liter of medium and ampicillin. After growing the bacteria until the optical density at 600 nm is 0.6-0.8, measured via spectrophotometer, IPTG was added to induce expression and the bacteria was incubated either overnight at 18°C or 6 hours at 37°C. Samples were taken before and after induction for western blot tests. The cells were then pelletized via centrifugation and stored at -80°C. In addition to the Aurora B-INCENP plasmids, unmodified pET-16b was used as a positive control to GST antibody blots and PreScission protease was transformed and expressed to be used in the following purification.

The western blot samples were centrifuged and lysed with a buffer containing sodium dodecyl sulphate and β-mercaptoethanol. The samples were then boiled for 5 min and stored at -20°C. The western blot used a 4-12% Bis-Tris gel with a MOPS running buffer. After loading the samples, marker buffer, and GST as positive control into the wells of the gel, 200V was applied to electrophorese the protein down the gel. The gel was then split into two: half was electrophoretically transferred to an activated PVDF

membrane, and the other half was stained with Coomassie blue and agitated. The PVDF membrane was blocked with a buffer of milk and TBS-Tween, then agitated overnight with a mixture of the buffer with primary antibodies, either GST-specific or Aurora B-specific, at 4°C. The gel in Coomassie blue was then placed in destainer, left overnight, and imaged using an ImageQuant LAS 400. After agitating overnight, the membrane was washed in TBS-Tween buffer and milk buffer was added along with secondary antibodies, of which type depended on the source of the primary antibodies, then agitated. The mixture was poured out and the membrane was agitated with TBS-Tween, then was washed with the combination of oxidizing and luminol reagents before imaging.

Purification

Following expression, the pelletized cells were lysed in a buffer containing Tris, EDTA, DTT, β-mercaptoethanol, PMSF-Benz, Leupeptin, and Triton-X100 and sonicated in ice water for 30 min. The lysate was then centrifuged and the supernatant was sampled and pour into falcon tubes. Glutathione agarose (Sepharose) beads which have been swollen overnight in DI water were added along with buffer containing the solutions described above without Triton-X100. After incubating at 4°C, the mixture was poured into a filtered column with a sample taken from the flowthrough. The tubes were then washed with buffer and poured into the column with another sample taken. An elution buffer containing reduced glutathione was poured into the column with multiple microcentrifuge tubes used to catch the eluted product. The protein concentration in each tube was initially tested via NanoDrop before dialysis via microfiltration tubes at 4°C overnight.

Bradford assays were performed to quantify protein amount. A range of volumes of bovine serum albumin and different elution fractions were each mixed with Bradford reagent and agitated. Optical density at 595 nm was measured for each solution and the slope of the constructed calibration curve was used to calculate protein concentration of the fractions.

The protein amount was also quantified via Coomassie gel. A range of volumes of bovine serum albumin protein, a range of serial dilutions of combined eluted protein solution, and marker solution were added to different wells of a gel. The procedure followed was the same as described in the Transformation + Expression section above. Quantification of the resulting bands was performed by image analysis using ImageJ.

10. References

1. McIntosh, J. R. (1989). Mitosis. *Science*, 246(4930), 622–628.
2. Tyson, J. J., Csikasz-Nagy, A., & Novak, B. (2002). The dynamics of cell cycle regulation. *BioEssays*. doi.org/10.1002/bies.10191
3. Mcintosh, J. (2016). Mitosis. *Cold Spring Harbor Perspectives in Biology*, *8*(9). doi.org/10.1101/cshperspect.a023218
4. Gelens, L., Qian, J., Bollen, M., & Saurin, A. T. (2018). The importance of kinase–phosphatase integration: lessons from mitosis. *Trends in Cell Biology*, *28*(1), 6–21. doi.org/10.1016/j.tcb.2017.09.005
5. Kops, G. J. P. L., Saurin, A. T., & Meraldi, P. (2010). Finding the middle ground: How kinetochores power chromosome congression. *Cellular and Molecular Life Sciences*. doi.org/10.1007/s00018-010-0321-y
6. Broad, A. J., & DeLuca, J. G. (2020). The right place at the right time: Aurora B kinase localization to centromeres and kinetochores. *Essays in Biochemistry*, *64*(2), 299–311. doi.org/10.1042/ebc20190081
7. Gordon, D. J., Resio, B., & Pellman, D. (2012). Causes and consequences of aneuploidy in cancer. *Nature Reviews Genetics*. doi.org/10.1038/nrg3123
8. Krenn, V., & Musacchio, A. (2015). The Aurora B kinase in chromosome bi-orientation and spindle checkpoint signaling. *Frontiers in Oncology*, *5*. doi.org/10.3389/fonc.2015.00225
9. Gonze, D., & Goldbeter, A. (2001). A model for a network of phosphorylation-dephosphorylation cycles displaying the dynamics of dominoes and clocks. *Journal of Theoretical Biology*, *210*(2), 167–186. doi.org/10.1006/jtbi.2000.2294
10. Zaytsev, A. V, Segura-Peñ, D., Godzi, M., Calderon, A., Ballister, E. R., Stamatov, R., … Grishchuk, E. L. (2016). Bistability of a coupled Aurora B kinase-phosphatase system in cell division. *ELife*, *5*. doi.org/10.7554/eLife.10644.001
11. Carmena, M., Wheelock, M., Funabiki, H., & Earnshaw, W. C. (2012). The chromosomal passenger complex (CPC): From easy rider to the godfather of mitosis. *Nature Reviews Molecular Cell Biology*, *13*(12), 789–803. doi.org/10.1038/nrm3474
12. Willems, E., Dedobbeleer, M., Digregorio, M., Lombard, A., Lumapat, P. N., & Rogister, B. (2018). The functional diversity of Aurora kinases: A comprehensive review. *Cell Division*, *13*(1). doi.org/10.1186/s13008-018-0040-6
13. Fuller, B. G., Lampson, M. A., Foley, E. A., Rosasco-Nitcher, S., Le, K. V., Tobelmann, P., … Kapoor, T. M. (2008). Midzone activation of aurora B in anaphase produces an intracellular phosphorylation gradient. *Nature*, *453*(7198), 1132–1136. doi.org/10.1038/nature06923

14. Tan, L., & Kapoor, T. M. (2011). Examining the dynamics of chromosomal passenger complex (CPC)-dependent phosphorylation during cell division. *Proceedings of the National Academy of Sciences*, *108*(40), 16675–16680. doi.org/10.1073/pnas.1106748108

15. Chen, G. Y., Renda, F., Zhang, H., Gokden, A., Wu, D. Z., Chenoweth, D. M., … Lampson, M. A. (2021). Tension promotes kinetochore-microtubule release by Aurora B kinase. *The Journal of Cell Biology*, *220*(6). doi.org/10.1083/jcb.202007030

16. Kelly, A. E., Sampath, S. C., Maniar, T. A., Woo, E. M., Chait, B. T., & Funabiki, H. (2007). Chromosomal enrichment and activation of the Aurora B pathway are coupled to spatially regulate spindle assembly. *Developmental Cell*, *12*(1), 31–43. doi.org/10.1016/j.devcel.2006.11.001

17. Wang, E., Ballister, E. R., & Lampson, M. A. (2011). Aurora B dynamics at centromeres create a diffusion-based phosphorylation gradient. *Journal of Cell Biology*, *194*(4), 539–549. doi.org/10.1083/jcb.201103044

18. Sessa, F., Mapelli, M., Ciferri, C., Tarricone, C., Areces, L. B., Schneider, T. R., … Musacchio, A. (2005). Mechanism of Aurora B activation by INCENP and inhibition by hesperadin. *Molecular Cell*, *18*(3), 379–391. doi.org/10.1016/j.molcel.2005.03.031

19. Silverman, A. D., Karim, A. S., & Jewett, M. C. (2020). Cell-free gene expression: an expanded repertoire of applications. *Nature Reviews Genetics*, *21*(3), 151–170. doi.org/10.1038/s41576-019-0186-3

20. Ferrell, J. E. (2002). Self-perpetuating states in signal transduction: Positive feedback, double-negative feedback and bistability. *Current Opinion in Cell Biology*, *14*(2), 140–148. doi.org/10.1016/S0955-0674(02)00314-9

21. Rulands, S., Klünder, B., & Frey, E. (2013). Stability of localized wave fronts in bistable systems. *Physical Review Letters*, *110*(3). doi.org/10.1103/PhysRevLett.110.038102

22. Lisman, J. E. (1985). A mechanism for memory storage insensitive to molecular turnover: A bistable autophosphorylating kinase. *Neurobiology*, *82*, 3055–3057.

23. Cherry, J. L., & Adler, F. R. (2000). How to make a biological switch. *Journal of Theoretical Biology*, *203*(2), 117–133. doi.org/10.1006/jtbi.2000.1068

24. Ferrell, J. (1996). Tripping the switch fantastic: how a protein kinase cascade can convert graded inputs into switch-like outputs. *Trends in Biochemical Sciences*, *21*(12), 460–466.

25. Ferrell, J. E. (2012). Bistability, bifurcations, and Waddington's epigenetic landscape. *Current Biology*, *22*(11). doi.org/10.1016/j.cub.2012.03.045

26. pGEX vectors. Sigma Aldrich. https://www.sigmaaldrich.com/BE/en/technical-documents/protocol/genomics/cloning-and-expression/pgex-vectors

27. Hanahan, D., Jessee, J., & Bloom, F. R. (1991). Plasmid transformation of Escherichia coli and other bacteria. *Methods in Enzymology*, *204*(C), 63–113. doi.org/10.1016/0076-6879(91)04006-A

28. Elkins, J. M., Santaguida, S., Musacchio, A., & Knapp, S. (2012). Crystal structure of human aurora B in complex with INCENP and VX-680. *Journal of Medicinal Chemistry*, *55*(17), 7841–7848. doi.org/10.1021/jm3008954

29. Adams, R. R., Wheatley, S. P., Gouldsworthy, A. M., Kandels-Lewis, S. E., Carmena, M., Smythe, C., … Earnshaw, W. C. (2000). INCENP binds the Aurora-related kinase AIRK2 and is required to target it to chromosomes, the central spindle and cleavage furrow. *Current Biology*, *10*(17), 1075–1078.

30. Ninfa, A. J., Ballou, D. P., & Benore, M. (2009). *Fundamental laboratory approaches for biochemistry and biotechnology*. 161-172. John Wiley & Sons.

31. Harper, S., & Speicher, D. W. (2011). Purification of proteins fused to glutathione S-transferase. *Methods in Molecular Biology*, *681*, 259–280. doi.org/10.1007/978-1-60761-913-0_14

32. Goldring, J. P. D. (2019). Measuring protein concentration with absorbance, lowry, bradford coomassie blue, or the smith bicinchoninic acid assay before electrophoresis. In *Electrophoretic separation of proteins: methods and protocols* (pp. 31–39). Retrieved from www.springer.com/series/7651

33. Alonso Villela, S. M., Kraïem, H., Bouhaouala-Zahar, B., Bideaux, C., Aceves Lara, C. A., & Fillaudeau, L. (2020). A protocol for recombinant protein quantification by densitometry. *MicrobiologyOpen*, *9*(6), 1175–1182. doi.org/10.1002/mbo3.1027

34. Tsai, J. C., Zhang, W., Kirk, V., & Sneyd, J. (2012). Traveling waves in a simplified model of calcium dynamics. *SIAM Journal on Applied Dynamical Systems*, *11*(4), 1149–1199. doi.org/10.1137/120867949

35. Pinto, D. J., Bard Ermentrout, G., & Appl Math, S. J. (2001). Spatially structured activity in synaptically coupled neuronal networks: I. Traveling fronts and pulses. *Society for Industrial and Applied Mathematics*, *62*(1), 206–225. Retrieved from epubs.siam.org/page/terms

36. Barton, N. H., & Turelli, M. (2011). Spatial waves of advance with bistable dynamics: cytoplasmic and genetic analogues of Allee effects. *American Naturalist*, *178*(3). doi.org/10.1086/661246

37. Van Saarloos, W. (1988). Front propagation into unstable states: marginal stability as a dynamical mechanism for velocity selection. *Physical Review A*, *37*(1), 211–229. doi.org/10.1103/PhysRevA.37.211

38. Liu, D., Vader, G., Vromans, M., Lampson, M., & Lens, S. (2009). Sensing chromosome bi-orientation by spatial separation of Aurora B kinase from kinetochore substrates. *Science*, *323*(5919), 1350–1353. doi.org/10.1126/science.1167396

39. Mori, Y., Jilkine, A., & Edelstein-Keshet, L. (2008). Wave-pinning and cell polarity from a bistable reaction-diffusion system. *Biophysical Journal*, *94*(9), 3684–3697. doi.org/10.1529/biophysj.107.120824

40. Bhattacharya, S., Banerjee, T., Miao, Y., Zhan, H., Devreotes, P. N., & Iglesias, P. A. (2020). Traveling and standing waves mediate pattern formation in cellular protrusions. *Sci. Adv*, *6*, 7682–7689. Retrieved from advances.sciencemag.org/

41. Knobloch, E. (2015). Spatial localization in dissipative systems. *Annual Review of Condensed Matter Physics*, *6*(1), 325–359. doi.org/10.1146/annurev-conmatphys-031214-014514

42. Champneys, A. R., Al Saadi, F., Breña-Medina, V. F., Grieneisen, V. A., Marée, A. F. M., Verschueren, N., & Wuyts, B. (2021). Bistability, wave pinning and localisation in natural reaction–diffusion systems. *Physica D: Nonlinear Phenomena*, *416*. doi.org/10.1016/j.physd.2020.132735

43. Fife, P. C., & Mcleod, J. B. (1977). The approach of solutions of nonlinear diffusion equations to travelling front solutions. *Archive for Rational Mechanics and Analysis*, *65*(4), 335–361.

44. Rombouts, J., & Gelens, L. (2021). Dynamic bistable switches enhance robustness and accuracy of cell cycle transitions. *PLoS Computational Biology*, *17*(1). doi.org/10.1371/JOURNAL.PCBI.1008231

45. Liu, D., Vleugel, M., Backer, C. B., Hori, T., Fukagawa, T., Cheeseman, I. M., & Lampson, M. A. (2010). Regulated targeting of protein phosphatase 1 to the outer kinetochore by KNL1 opposes Aurora B kinase. *Journal of Cell Biology*, *188*(6), 809–820. doi.org/10.1083/jcb.201001006

46. Nasa, I., Rusin, S. F., Kettenbach, A. N., & Moorhead, G. B. (2018). Aurora B opposes PP1 function in mitosis by phosphorylating the conserved PP1-binding RVxF motif in PP1 regulatory proteins. *Sci. Signal*, *11*(530), 8669. Retrieved from stke.sciencemag.org/

47. Brauns, F., Halatek, J., & Frey, E. (2020). Phase-space geometry of mass-conserving reaction-diffusion dynamics. *Physical Review X*, *10*(4). doi.org/10.1103/PhysRevX.10.041036

48. Breña-Medina, V., & Champneys, A. (2014). Subcritical turing bifurcation and the morphogenesis of localized patterns. *Physical Review E*, *90*(3). doi.org/10.1103/PhysRevE.90.032923

AFDELING
Straat nr bus 0000
3000 LEUVEN, BELGIË
tel. + 32 16 00 00 00
fax + 32 16 00 00 00
www.kuleuven.be